Macromolecules

pubs.acs.org/Macromolecules Article

Rheological Scaling of Ionic Liquid-Based Polyelectrolytes in the Semidilute Unentangled Regime from Low to High Salt Concentrations

Atsushi Matsumoto,* Ryota Yoshizawa, Osamu Urakawa, Tadashi Inoue, and Amy Q. Shen*

Cite This: *Macromolecules* 2021, 54, 5648−5661 Read Online

ABSTRACT: Polymerized ionic liquids (PILs) are a special class of ion-containing polymers with ionic liquid structures. The viscoelastic properties of PILs in IL solutions are expected to be influenced by both polymer−polymer interaction and charge screening by IL ions, which becomes complex at high IL concentrations due to strong ionic correlations. In this work, we aim to understand the effect of the ionic correlations on the shear rheology of PIL in IL solutions in the semidilute unentangled (SU) polymer regime, with moderate polymer−polymer interactions. We conducted systematic rheological characterization of a PIL, poly(1-butyl-3-vinylimidazolium bis(trifluoromethanesulfonyl)imide), in a mixture of an IL, 1-butyl-3-methylimidazolium bis(trifluoromethanesulfonyl)imide, and a non-ionic solvent, dimethylformamide, to evaluate the specific viscosity η_{sp} and the longest relaxation time λ with varying IL concentrations c_{IL}, at a fixed polymer concentration. We found that both η_{sp} and λ initially decreased with the increasing c_{IL}, following the scaling theory of polyelectrolyte solutions in the low salt concentration regime. However, these values exhibited an upturn at high c_{IL}. We explained the observed non-monotonic viscoelastic behavior by proposing a charge screening model for SU solutions, accounting for both modified screening length in concentrated IL solutions and complete charge screening. Our results demonstrate how the strong ionic correlation in concentrated IL solutions modifies the electrostatics of PILs and their corresponding viscoelastic properties in the presence of moderate polymer−polymer interactions.

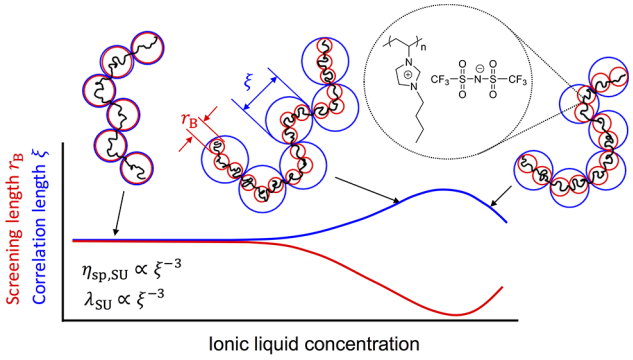

1. INTRODUCTION

Ionic liquids are organic molten salts in the liquid state.[1] Polymerized ionic liquids (PILs) are a special class of ion-containing polymers with ionic liquid structures being covalently attached to the repeating unit.[2−5] Because PILs combine the unique features of ILs (e.g., thermal/electrochemical stability)[6] with those of polymers (good mechanical properties), they have found wide applications as electrolytes in batteries,[7,8] membranes for molecular separation,[9] stabilizers for nanoparticles in solutions,[10] and lubricant additives for coating.[11] The performance of PILs can be further enhanced by using ILs as solvents to increase the mobility of PIL chains.[12−17] Consequently, the viscoelastic properties of PILs in solutions are critical to optimize PIL-based material design and performance.

The viscoelastic properties for ordinary ion-containing polymers [e.g., poly(sodium styrenesulfonate)] are governed by both ion−ion and polymer−polymer interactions.[13,18−33] In particular, their solution properties are influenced by the electrostatic interactions, which can be tuned by adjusting the amount of salt in the solution.[18] For example, zero shear viscosity becomes significantly larger for polyelectrolytes in comparison to the corresponding neutralized polyelectrolyte due to electrostatic repulsion.[22] At a fixed polymer concentration, zero shear viscosity decreases with increasing salt concentrations due to the charge screening.[29] The effect of the charge screening on viscoelastic properties of polyelectrolytes[20,27,28,34−37] has been captured by the scaling theory proposed by Dobrynin et al. on the basis of the Debye−Hückel (DH) theory for dilute solutions (see more details in Section S1).

However, the DH theory is expected to become inapplicable at high salt concentrations due to ion−ion interactions. Gebbie et al.[38] first experimentally examined the charge screening length in pure ILs using a surface force apparatus. By measuring the separation force generated by an IL confined between two charged plates, they observed that the long-range

Received: March 14, 2021
Revised: May 4, 2021
Published: June 1, 2021

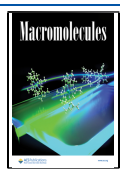

https://doi.org/10.1021/acs.macromol.1c00576
Macromolecules 2021, 54, 5648−5661

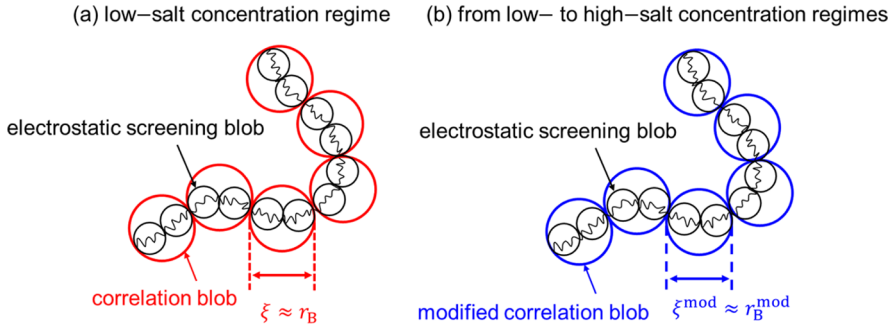

Figure 1. (a) Conformation of a polyelectrolyte chain in a SU solution proposed by Dobryinin et al.[20] The polyelectrolyte chain is assumed to be a random walk of correlation blobs with length ξ consisting of multiple electrostatic screening blobs. In the low-salt limit, the correlation length ξ is on the order of the screening length r_B, that is, $\xi \approx r_B$ for $2Ac_{salt}/c_p \ll 1$. (b) In the proposed charge screening model, a modified polyelectrolyte chain in the SU regime is a random walk of modified correlation blobs with length ξ^{mod}, consisting of multiple modified electrostatic screening blobs.

force decayed exponentially over distance. The characteristic decay length (much larger than the value predicted by the DH theory) was considered as the screening length in the IL. Similar long-range exponential decay of separation forces, therefore larger screening lengths, have been confirmed by several experimental[39−44] and theoretical[45−51] studies for both ILs and ordinary salts. Moreover, the ionic correlation effect on the charge screening is found to become more important for salts having large ion diameters, such as ILs.[41]

Motivated by the above observation, we recently examined the viscoelastic properties of PIL (PC_4-TFSI) in a mixture of a non-ionic solvent [dimethylformamide (DMF)] and an IL [1-butyl-3-methylimidazolium bis(trifluoromethanesulfonyl)imide (Bmim-TFSI)] in the dilute (DL) polymer regime, where the polymer−polymer interactions were essentially negligible.[23] By measuring the specific viscosity η_{sp} and the longest relaxation time λ (related to the end-to-end distance of PIL chains in the DL regime) of this solution, we found that both η_{sp} and λ decreased with increasing IL concentrations c_{IL} due to the charge screening effect at low c_{IL}, reached a minimum, but increased again at higher c_{IL} due to strong ionic correlations.[23] Because the end-to-end distance of PIL chains, the characteristic length in the DL regime, is related to the screening length, we proposed a modified scaling theory by introducing a modified screening length in concentrated IL solutions (see more details in Section S4), showing good agreement with the observed non-monotonic dependence of η_{sp} and λ on c_{IL} in the DL regime.[23,41,42]

When the polymer concentration is increased to reach the semidilute unentangled (SU) regime, polymer chains in solutions are no longer isolated and start to overlap with each other. This concentration regime is very important for polymer-processing operations such as high-speed coating, as moderate elasticity of the solution is required.[13,17,22] In the SU regime, the dynamics of polymer chains is affected by the partial screening of the hydrodynamic interactions by the intermolecular interactions,[52] and the correlation blob is introduced as a characteristic length to describe the viscoelastic properties of SU polymer solutions.[52] For ordinary polyelectrolyte solutions in the SU regime, Dobrynin et al.[20] showed that the concept of correlation blobs was still applicable, but its length was influenced by the electrostatic interactions, analogous to the end-to-end distance of polyelectrolytes in the DL regime (see Figure 1). However, we anticipate that at high IL concentrations in the SU regime, the electrostatic interactions between IL ions would affect the correlation length of PIL chains in a different manner from those predicted by Dobrynin's scaling theory.[20]

In this work, we investigate whether the viscoelastic properties of PILs in IL solutions in the SU regime can be captured by the scaling laws of Dobrynin et al.[20] over the full IL concentration range. We measure η_{sp} and λ at a fixed PIL concentration c_p while varying the IL concentration until it reaches its saturation value, that is, the concentration of pure IL. Our results show that both η_{sp} and λ decrease initially with increasing IL concentrations in the low IL concentration regime, in good agreement with the scaling predictions by Dobrynin et al. for ordinary polyelectrolyte solutions in the SU regime. However, a significant deviation from Dobrynin's scaling predictions is observed for both η_{sp} and λ in the high IL concentration regime: both values first reach a minimum but exhibit an upturn when the IL concentration is increased further. We explain this discrepancy by proposing a charge screening model for SU solutions, accounting for both the modified screening length in concentrated IL solutions and complete charge screening.

2. EXPERIMENTAL SECTION

2.1. Materials. 1-Vinylimidazole was purchased from Tokyo Chemical Industry and used after distillation at 85 °C under vacuum. Lithium bis(trifluoromethanesulfonyl)imide (Li-TFSI), 1-bromobutane, 2,2′-azobis(isobutyronitrile) (AIBN), and super dehydrated DMF were purchased from Wako Pure Chemicals. Silver nitrate ($AgNO_3$) at 0.1 M in an aqueous solution was purchased from Sigma-Aldrich. Bmim-TFSI (Purity > 99.5%) was purchased from Ionic Liquid Technologies. Deuterated water was purchased from Merck and used as a solvent for NMR measurements. After passing through a Q-POD Element unit (Merck Millipore), Milli-Q water with a resistivity higher than 18.2 MΩ cm was used as a solvent.

2.2. Synthesis of PILs. The monomer 1-butyl-3-vinylimidazolium bromide (C_4−Br) was first prepared by quaternizing 1-vinylimidazole with 1-bromobutane. After removing the unreacted 1-vinylimidazole and 1-bromobutane, the polymerization of C_4−Br was carried out by using AIBN as an initiator in Milli-Q water. The purity of C_4−Br was confirmed by ^{1}H NMR in deuterated water at 25 °C. The peak chemical shifts in δ (ppm) were: 8.9 (1H, s, N−C*H*═N), 7.6 (1H, d, N−CH═C*H*−N−Bu), 7.4 (1H, d, N−C*H*═CH−N−Bu), 7.0 (1H, q, CH_2═C*H*−N), 5.6 (1H, dd, trans−CH_2═CH−N), 5.2 (1H, dd, cis−CH_2═CH−N), 4.1 (2H, t, N−CH_2−CH_2−CH_2−CH_3), 1.7 (2H, m, N−CH_2−CH_2−CH_2−CH_3), 1.2 (2H, m, N−CH_2−CH_2−CH_2−CH_3), 0.7 (3H, t, N−CH_2−CH_2−CH_2−CH_3). Here, "*H*" denotes the proton corresponding to each peak chemical shift.

https://doi.org/10.1021/acs.macromol.1c00576
Macromolecules 2021, 54, 5648−5661

Poly(1-butyl-3-vinylimidazolium bromide (PC_4−Br) was prepared via free radical polymerization of the C_4−Br. The polymerization was initiated by AIBN at 60 °C for 16 h in Milli-Q water. The molar ratio of the monomer to the initiator was set as 100. After polymerization, PC_4−Br was dialyzed against Milli-Q water for 1 week using a dialysis tube (Fisher Scientific, Ltd.) with a nominal molecular weight cut-off at 6000−8000 Da. During the dialysis, the Milli-Q water was refreshed daily. The resultant solution was then dried via a freeze-drying method, and PC_4−Br was obtained in a powder form and stored under vacuum before usage.

Poly(1-butyl-3-vinylimidazoliumbis(trifluoromethanesulfonyl)-imide) (PC_4-TFSI) was prepared by using the counterion conversion method proposed by Mecerreyes et al.[53] Specifically, an aqueous solution containing Li-TFSI was slowly titrated into an aqueous solution containing PC_4−Br, and the mixture was stirred for 3 days at room temperature. The molar ratio of the Li-TFSI to the monomer was 1.5. During this process, bromide counteranions were replaced with TFSI anions, and PC_4-TFSI was precipitated. The precipitate was then washed with Milli-Q water until the filtrate remained transparent when adding an aqueous solution containing 0.1 M $AgNO_3$. PC_4-TFSI was finally obtained in a powder form.

2.3. Preparation of the Test Mixtures. Test mixtures consisted of PIL (PC_4-TFSI) in a solvent mixture of the IL (Bmim-TFSI) and a non-ionic solvent (DMF). The Bmim-TFSI acts as both a solvent and the source of salt ions to regulate the electrostatic screening. Test mixtures were prepared by using two different methods, depending on the concentration of PC_4-TFSI and Bmim-TFSI in DMF. At high concentrations of PC_4-TFSI and Bmim-TFSI, test mixtures were prepared by directly adding the components into a glass vial. At low concentrations of PC_4-TFSI and Bmim-TFSI, test mixtures were prepared by diluting concentrated solutions of PC_4-TFSI and Bmim-TFSI. The concentration of Bmim-TFSI, c_{IL}, was calculated as $c_{IL} = m_{IL}\rho/M_0 m_{tot}$, where ρ and $M_0 = 419.36$ g mol^{-1} are the density of the solvent mixture[23] and the molar mass of Bmim-TFSI, respectively, while m_{IL} and m_{tot} are the mass of Bmim-TFSI and the mass of the mixture of DMF and Bmim-TFSI, respectively. Note that the density of the solvent mixture varies with the Bmim-TFSI concentration c_{IL}, ranging from 0 M (pure DMF) to 3.42 M (pure Bmim-TFSI), as shown in Figure S8 of the Supporting Information. The monomer concentration of PC_4-TFSI, c_p, was calculated as the ratio of the number of moles of the repeating unit of PC_4-TFSI to the volume of the mixture of DMF and Bmim-TFSI: $c_p = m_p\rho/M_r m_{tot}$, where m_p is the mass of PC_4-TFSI, and $M_r = 431.43$ g mol^{-1} is the molar mass of the repeating unit associated with the counteranion. Because DMF is a hygroscopic solvent, sample preparation was conducted in a glovebox under an argon atmosphere. The prepared solutions were hermetically sealed in borosilicate glass vials and then stored in a desiccator while maintaining humidity lower than 20% until use.

2.4. Shear Viscosity and Complex Shear Modulus Measurements. The shear viscosity η at 25 °C was measured using a strain-controlled rheometer ARES-G2 (TA Instruments) by varying the shear rate $\dot{\gamma}$ from 0.01 to 1,000 s^{-1}. A stainless steel cone and plate geometry with 50 mm in diameter and 1° in cone angle was used as an upper geometry, while a stainless steel flat plate with 60 mm in diameter was attached into an advanced Peltier system (TA Instruments) as a lower geometry to regulate temperature with a temperature accuracy of ±0.1 °C. The loaded solution was covered with a solvent trap to prevent both moisture absorption from the ambient environment and the sample evaporation.

The same rheometer, fixtures, and the solvent trap were used to measure the complex shear modulus $G^*(= G' + iG'')$ in the frequency range of $0.1 \leq \omega \leq 100$ rad s^{-1} at 25 °C. The shear strain γ was set at 3% for high-viscosity solutions and 10% for low-viscosity solutions to ensure the linear regime where the value of G^* is independent of γ.[54]

2.5. Dielectric Constant Measurements. The complex permittivity ε^* $(= \varepsilon' - i\varepsilon'')$ in a frequency range 1 MHz $\leq f \leq$ 3 GHz was measured using a RF LCR meter (4287A, Agilent Technologies) equipped with a homemade stainless steel electrode cell. The instrument was calibrated using an ultrapure water (Wako pure Chemicals). The vacant electric capacitance C_0 was measured without samples and obtained as $C_0 = 0.23$ pF. After loading a test sample in the cell, the experiment was performed at room temperature (~25 °C), and the electric capacitance C and conductance G of the sample as a function of frequency f were determined using a parallel connected equivalent circuit model. The real and imaginary parts of the complex permittivity were then calculated as $\varepsilon' = CC_0^{-1}$ and $\varepsilon'' = G(2\pi C_0 f)^{-1}$, respectively.

3. SCALING THEORY OF POLYELECTROLYTE SOLUTIONS IN THE SU REGIME AT LOW SALT CONCENTRATIONS

Existing scaling theories discuss the effect of the electrostatics on the polyelectrolyte conformation in solutions.[20,21,55−58] In particular, the scaling analysis by Dobrynin et al.[20] has matched many experimental results well for polyelectrolyte solutions in the SU polymer regime.[13,28−30,59−62] Accordingly, we review their scaling theory for polyelectrolytes in good solvents in the SU regime.[20]

Dobrynin et al. applied the DH theory to predict the viscoelastic properties of polyelectrolyte solutions in the presence of salts. Specifically, the scaling law involves the conformation parameters of polyelectrolytes, such as the end-to-end distance R for the dilute (DL) regime, and the correlation length ξ for the SU regime, while these conformation parameters are functions of the screening length. According to the DH theory, the Debye screening length r_{Debye} is given by

$$r_{Debye} = \left[\frac{4000\pi N_A l_B c_p}{A}\left(1 + \frac{2Ac_{salt}}{c_p}\right)\right]^{-1/2} \tag{1}$$

where N_A, A, and c_{salt} are the Avogadro constant, the number of monomers between uncondensed charges, and the total molar concentration of salts. Here, $l_B = e^2/4\pi\varepsilon_r\varepsilon_0 k_B T$ is the Bjerrum length, where e, ε_r, ε_0, k_B, and T are the elementary charge, the dielectric constant of solvent mixture, the dielectric constant of vacuum, the Boltzmann constant, and the absolute temperature. The parameter A characterizes the number of dissociated ions on a polyelectrolyte chain, which depends on the type of polyelectrolytes and solvents.[20,60] Dobrynin et al. argued that a screening length r_B larger than r_{Debye} was required to screen ions on the polyelectrolyte chain

$$r_B = \left[\frac{1000 N_A b c_p}{B}\left(1 + \frac{2Ac_{salt}}{c_p}\right)\right]^{-1/2} \tag{2}$$

where b is the monomer size and $B = (bA^2/l_B)^{2/7}$ is the dimensionless contour length parameter.

Figure 1a depicts the conformation of a polyelectrolyte in a good solvent in the SU regime, proposed by Dobrynin et al.[20] The polyelectrolyte chain is assumed to be a random walk of correlation blobs with length ξ, consisting of multiple electrostatic screening blobs. The scaling law of the correlation length ξ of the polyelectrolyte chain was derived using the general scaling assumption[20]

$$\xi \propto \left(\frac{B}{b}\right)^{3/4} c_p^{-3/4} (r_B)^{-1/2} = \left(\frac{B}{b}\right)^{1/2} c_p^{-1/2}\left(1 + \frac{2Ac_{salt}}{c_p}\right)^{1/4} \tag{3}$$

Equation 3 predicts that the correlation length on the order of the screening length in the low-salt limit, that is, $\xi \approx r_B$ for $2Ac_{salt}/c_p \ll 1$, increases monotonically with increasing c_{salt} at a

https://doi.org/10.1021/acs.macromol.1c00576
Macromolecules 2021, 54, 5648−5661

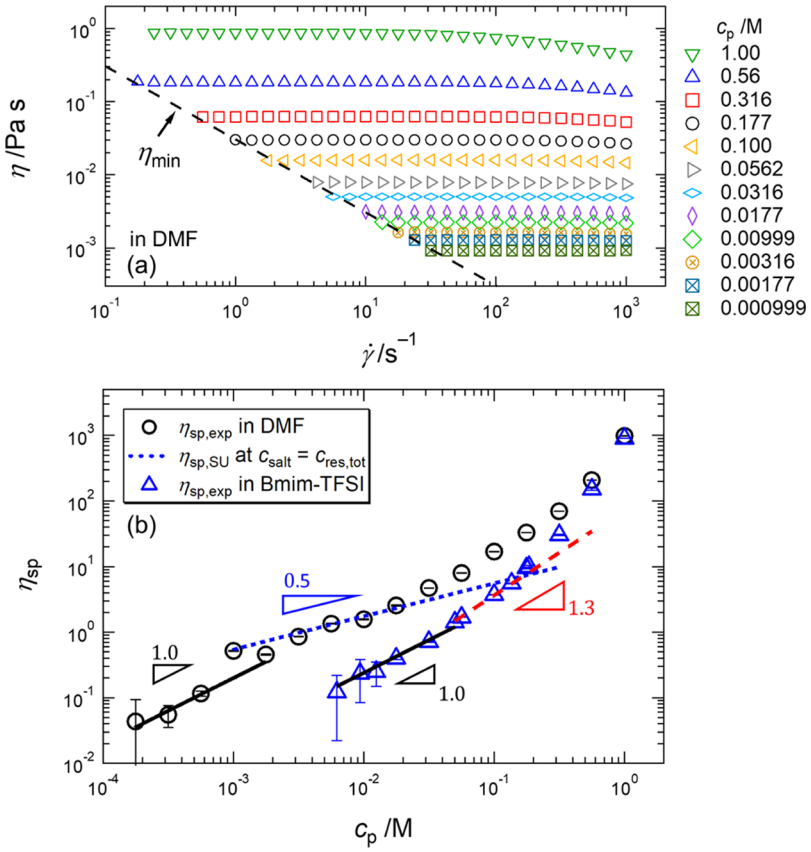

Figure 2. (a) Shear viscosity curves at 25 °C for PC_4-TFSI in non-ionic DMF at c_{IL} = 0 M with different monomer concentrations c_p. The dashed line indicates the minimum measurable shear viscosity η_{min} of the instrument.[23] (b) Dependence of the specific viscosity η_{sp} at 25 °C on the monomer concentration c_p for PC_4-TFSI at c_{IL} = 0 M in DMF (black circles) and at c_{IL} = 3.42 M in pure Bmim-TFSI (blue triangles). The blue-dotted line is plotted based on eq 4 for $\eta_{sp,SU}$ at A = 2 and $c_{salt} = c_{res,tot} = (9.24 \times 10^{-6} + 0.009c_p)$ M. The power-law fits of the measured η_{sp} for dilute and SU regimes are represented as black solid- and red-dashed lines, respectively. The error bars of η_{sp} were originated from the experimental errors of shear viscosity η.

fixed c_p. The scaling law of the specific viscosity η_{sp} and the longest relaxation time λ in the SU regime was then derived using the Rouse−Zimm model

$$\eta_{sp,SU} \propto N c_p^{-1} \xi^{-3} \propto N \left(\frac{b}{B}\right)^{3/2} c_p^{1/2} \left(1 + \frac{2Ac_{salt}}{c_p}\right)^{-3/4} \quad (4)$$

$$\lambda_{SU} \propto \eta_s N^2 c_p^{-2} \xi^{-3} \propto \eta_s N^2 \left(\frac{b}{B}\right)^{3/2} c_p^{-1/2} \left(1 + \frac{2Ac_{salt}}{c_p}\right)^{-3/4} \quad (5)$$

where η_s is the solvent viscosity. Equations 4 and 5 predict a monotonic decrease of η_{sp} and λ/η_s at a fixed c_p in the SU regime with increasing c_{salt}.

4. RESULTS AND DISCUSSION

4.1. PC_4-TFSI in Non-Ionic DMF. The viscoelastic properties of polyelectrolytes in non-ionic solvents are sensitive to salt residues present in the system.[21] Here, the residual salt concentration is estimated as $c_{res,tot} = (9.24 \times 10^{-6} + 0.009c_p)$ M, by considering contributions from both solvent and polyelectrolyte samples (see details in Section S2). The total salt concentration c_{salt} in the solution is thus given by $c_{salt} = c_{IL} + c_{res,tot}$.

We measured the shear viscosity η of the PIL as a function of shear rate $\dot{\gamma}$ in non-ionic DMF (c_{IL} = 0 M), at various monomer concentrations c_p ranging from 1.0×10^{-3} to 1.0 M, shown in Figure 2a. The measured η below the minimum measurable shear viscosity η_{min} (dashed line) of the instrument was removed.[54] The values of η increased with increasing c_p in general. For a fixed c_p, η remained as a constant at low $\dot{\gamma}$, but started to decrease above a critical shear rate, exhibiting typical shear-thinning behavior for polymer solutions.

To determine polymer concentration regimes of the PIL in DMF, we plotted the specific viscosity $\eta_{sp} = \eta_0 - \eta_s/\eta_s$ as a function of c_p, shown as black circles in Figure 2b, with η_s the solvent viscosity. The zero-shear viscosity of the polymer solution η_0 was estimated by averaging the shear viscosity data in Figure 2a over shear rates, where η was independent of $\dot{\gamma}$ at low $\dot{\gamma}$. In Figure 2b, the specific viscosity for $c_{IL} < 3.0 \times 10^{-3}$ M increased linearly with increasing c_p until its value reached $\eta_{sp} = 1$ at $c_p \approx 3.0 \times 10^{-3}$ M. The obtained power-law exponent of $\eta_{sp}(\propto c_p^{1.0})$ agreed well with the general scaling exponent for dilute polymer solutions.[52] Thus, the overlap concentration c_p*of the PC_4-TFSI in DMF was determined as $c_p^* = 3.0 \times 10^{-3}$ M. Above the overlap polymer concentration, the tested solution enters typically to the SU regime. For $3.0 \times 10^{-3} \leq c_p \leq 2.0 \times 10^{-2}$ M, η_{sp} in DMF increased with increasing c_p and scaled as $\eta_{sp} \propto c_p^{0.5}$, showing good agreement with Dobrynin's scaling prediction of $\eta_{sp,SU}$ shown as the blue-dotted curve in Figure 2b. The agreement between the experimental data and the theoretical prediction was also reported for SU solutions of PILs in DMF.[13] When $c_p > 2.0 \times$

https://doi.org/10.1021/acs.macromol.1c00576
Macromolecules 2021, 54, 5648−5661

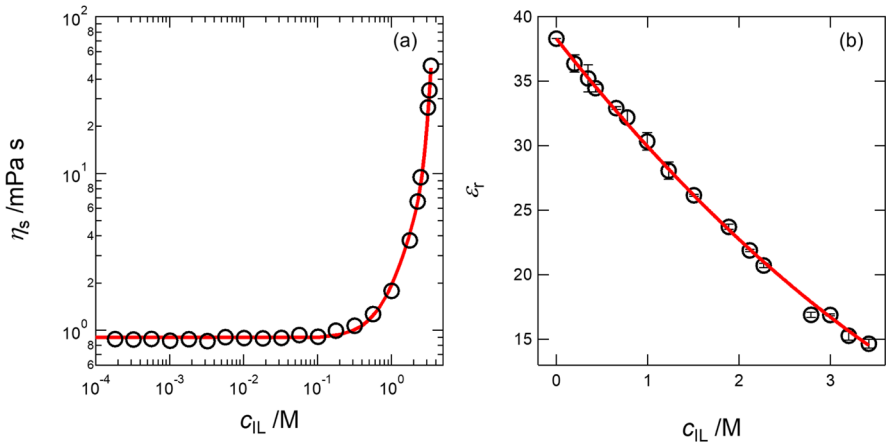

Figure 3. (a) Shear viscosity η_s of the solvent mixture of DMF and Bmim-TFSI at 25 °C is plotted as a function of the concentration of Bmim-TFSI c_{IL}. The measured η_s is fitted with a polynomial function (eq 13), and the best fit (red solid curve) is given by $B = 0.11\ M^{-1}$, $D = 1.1\ M^{-2}$, and $E = 1.8 \times 10^{-4}\ M^{-10}$. The error bars are smaller than the symbol size and therefore omitted in the plot. (b) Dielectric constant ε_r of the solvent mixture of DMF and Bmim-TFSI at 25 °C is plotted as a function of c_{IL}. The measured ε_r is fitted with a polynomial function (eq 14), and the best fit (red solid curve) is given by $G = -0.23\ M^{-1}$ and $H = 1.5 \times 10^{-2}\ M^{-2}$.

10^{-2} M, the specific viscosity increased more rapidly with increasing c_p, suggesting usually the transition from the SU to semidilute entangled or concentrated regimes.[32,63] However, by performing additional microrheology measurements, we confirmed that entanglements were not formed for the PC_4-TFSI in DMF at $c_p = 1$ M, and thus the viscoelastic properties of PC_4-TFSI solutions for $3.0 \times 10^{-3} < c_p < 1$ M should be captured by the scaling laws of SU solutions (see more details in Section S3). Nevertheless, a similar discrepancy between the measured η_{sp} and Dobrynin's scaling prediction of $\eta_{sp,SU}$ was reported for several polydisperse polyelectrolytes in pure water with negligible salt residues.[23,27,32,34,36,61,64−74] Although we do not have definitive interpretation, we speculate that the polydispersity of our PC_4-TFSI, synthesized via free radical polymerization, caused the discrepancy between the measured η_{sp} and its scaling prediction of $\eta_{sp,SU}$ at high c_p, leading to a more gradual transition of the polymer concentration regime.[27] We will not discuss this point further, but emphasize that the polydispersity of PC_4-TFSI will not influence the dependence of the specific viscosity and the longest relaxation time on the IL concentration at a fixed polymer concentration discussed in the following sections.

4.2. Proposed Charge Screening Model for Polyelectrolyte Solutions in the SU Regime: Low to High Salt Concentrations. When the salt concentration becomes sufficiently high, the scaling predictions of η_{sp} and λ shown in eqs 3−5 are expected to become inapplicable due to the breakdown of the DH theory.[41] Indeed, several research groups recently reported an unexpectedly large screening length in concentrated salt solutions, including both ionic liquids and ordinary salts.[38,39,41−44,46] In particular, Smith et al.[41] showed that the screening length in the low-salt concentration regime decreased with increasing salt concentrations, consistent with the DH prediction. With a further increase in the salt concentration, the screening length reached a minimum, followed by an upturn due to strong ionic correlations at high salt concentrations. The same group proposed a modified scaling law of the Debye screening length r_{Debye}^{mod} for electrolyte solutions[42]

$$r_{Debye}^{mod} \sim r_{Debye}\left(1 + \frac{a^3}{r_{Debye}^{\ 3}}\right) \tag{6}$$

where a is the salt ion diameter.

We assume that eq 6 holds for polyelectrolyte solutions. In this case, a modified scaling law of the screening length r_B^{mod} for polyelectrolyte solutions can be obtained by replacing r_{Debye} above with r_B

$$r_B^{mod} \sim r_B\left(1 + \frac{a^3}{r_B^{\ 3}}\right) \tag{7}$$

Following the same approach we conducted for DL solutions (see details in Section S4),[23] we derive the modified scaling law of the correlation length by simply replacing the screening length r_B in eq 3 with the modified screening length r_B^{mod} in eq 7

$$\xi^{mod} \propto \left(\frac{B}{b}\right)^{3/4} c_p^{\ -3/4}(r_B^{mod})^{-1/2} \tag{8}$$

On the basis of the Rouse−Zimm model, the modified scaling laws of the specific viscosity $\eta_{sp,SU}^{mod}$ and the longest relaxation time λ_{SU}^{mod} can be rewritten using ξ^{mod} in eq 8

$$\eta_{sp,SU}^{mod} \propto N c_p^{\ -1}(\xi^{mod})^{-3} \propto N\left(\frac{b}{B}\right)^{9/4} c_p^{\ 5/4}(r_B^{mod})^{3/2} \tag{9}$$

$$\lambda_{SU}^{mod} \propto \eta_s N^2 c_p^{\ -2}(\xi^{mod})^{-3} \propto \eta_s N^2\left(\frac{b}{B}\right)^{9/4} c_p^{\ 1/4}(r_B^{mod})^{3/2} \tag{10}$$

Bear in mind that the scaling law of ξ^{mod}, $\eta_{sp,SU}^{mod}$, and λ_{SU}^{mod} at low salt concentrations recovers Dobrynin's scaling law of ξ in eq 3, $\eta_{sp,SU}$ in eq 4, and λ_{SU} in eq 5, respectively.

Nevertheless, the modified scaling laws proposed above may not be sufficient to describe the viscoelastic properties of polyelectrolyte solutions due to complete charge screening at high salt concentrations. Specifically, polyelectrolyte chains in low-salt solutions are extended from their initial size due to electrostatic forces. With increasing salt concentrations, polyelectrolyte chains shrink and eventually reach the initial

https://doi.org/10.1021/acs.macromol.1c00576
Macromolecules 2021, 54, 5648−5661

polyelectrolyte chain size, that is, the charge effect can be screened completely at high salt concentrations. Indeed, several scattering[75,76] and viscosity[27,77−80] measurements showed an asymptotic decrease of properties with respect to increasing salt concentrations. Such an asymptotic behavior has been empirically captured by introducing a constant parameter in their corresponding properties,[78−85] corresponding to the size of polyelectrolytes in the absence of electrostatic interactions. Accordingly, we adjusted the modified scaling laws of $\eta_{sp,SU}^{mod}$ and λ_{SU}^{mod} by adding a constant parameter $\eta_{sp,SU}^{int}$ and λ_{SU}^{int}, denoting the intrinsic specific viscosity and the intrinsic longest relaxation time of polyelectrolyte solutions.

Finally, we propose a new charge screening model for the specific viscosity $\eta_{sp,SU}^{mod,int}$ and the longest relaxation time $\lambda_{SU}^{mod,int}$ of polyelectrolyte solutions in the SU regime as follows

$$\eta_{sp,SU}^{mod,int} = K_1 N \left(\frac{b}{B}\right)^{9/4} c_p^{5/4} (r_B^{mod})^{3/2} + \eta_{sp,SU}^{int} \tag{11}$$

$$\lambda_{SU}^{mod,int} = K_2 \eta_s N^2 \left(\frac{b}{B}\right)^{9/4} c_p^{1/4} (r_B^{mod})^{3/2} + \lambda_{SU}^{int} \tag{12}$$

where K_1 and K_2 are scaling prefactors.

4.3. PC_4-TFSI in the Mixture of DMF and Bmim-TFSI. We next investigated the charge screening behavior of PC_4-TFSI in the mixture of DMF and Bmim-TFSI in the SU regime by measuring the specific viscosity η_{sp} and the longest relaxation time λ while varying the Bmim-TFSI concentration c_{IL} at a fixed monomer concentration c_p. We tested five different c_p at (0.050, 0.100, 0.136, 0.185, and 0.250) M, all falling under the SU regime.

4.3.1. Effects of the Solvent Mixture. 4.3.1.1. Viscosity and Dielectric Constant. The original and our new charge screening models for SU solutions of polyelectrolytes predict that the specific viscosity (eqs 4 and 11) and the longest relaxation time (eqs 5 and 12) depend on the solvent viscosity η_s and the solvent dielectric constant ε_r. For the binary solvent of DMF and Bmim-TFSI, the values of η_s and ε_r can vary with c_{IL}.

Figure 3a shows the dependence of η_s at 25 °C on c_{IL}. The value of η_s was estimated by averaging shear viscosity η values of the solvent mixture at shear rates $\dot{\gamma}$ ranging from 0.1 to 1000 s^{-1}. The solvent viscosity increased monotonically with increasing c_{IL}, similar to the behavior observed for ionic liquids.[86−88] In particular, there is a drastic increase in η_s for c_{IL} > 1 M, suggesting the formation of ionic structures in the solvent mixture.[1] Thus, we expect that the longest relaxation time is significantly affected by the change of the solvent viscosity for c_{IL} > 1 M. We fitted the measured η_s as a function of c_{IL} using an empirical polynomial function

$$\eta_s = \eta_{DMF}(1 + Bc_{IL} + Dc_{IL}^2 + Ec_{IL}^{10}) \tag{13}$$

where $\eta_{DMF} = 8.8 \times 10^{-4}$ Pa s is the shear viscosity of DMF at 25 °C. The best fit is shown as the red solid curve in Figure 3a, corresponding to the fitting coefficients $B = 0.11\ M^{-1}$, $D = 1.1\ M^{-2}$, and $E = 1.8 \times 10^{-4}\ M^{-10}$.

Figure 3b shows the dependence of the dielectric constant ε_r at 25 °C on c_{IL}. The value of ε_r was estimated as the value of the real part of the complex permittivity ε' in the plateau regime at low frequencies, observed after subtracting the contribution of electrode polarization (see Section S5 in the Supporting Information for more details). We obtained ε_r = 38.3 for DMF and ε_r = 14.7 for Bmim-TFSI, also consistent with the literature values.[89,90] The dielectric constant decreased monotonically with increasing c_{IL} in the measured c_{IL} range, in good agreement with the literature report.[91] We fitted the measured ε_r as a function of c_{IL} using an empirical polynomial function

$$\varepsilon_s = \varepsilon_{r,DMF}(1 + Gc_{IL} + Hc_{IL}^2) \tag{14}$$

where $\varepsilon_{r,DMF}$ = 38.3 is the dielectric constant of DMF at 25 °C. The best fit is shown as the red solid curve in Figure 3b, corresponding to the fitting coefficients $G = -0.23\ M^{-1}$ and $H = 1.5 \times 10^{-2}\ M^{-2}$.

4.3.1.2. Solvent Quality. The solvent quality for a given polymer is controlled by the excluded volume of the polymer chain in a solvent determined by the balance between monomer−monomer and monomer−solvent attractions. The Flory exponent ν is commonly used to evaluate the solvent quality of a polymer for a given solvent.[52] According to Dobrynin's scaling theory for polyelectrolytes in good solvents, $\nu = 1$ is predicted for fully extended polyelectrolytes in the low-salt limit and $\nu = 0.6$ for coiled polyelectrolytes at high-salt limit, consistent with the value $\nu = 0.588$ predicted for electrically neutral polymers in good solvents.[52] Note that our proposed charge screening model also yields the same values of ν in both low- and high-salt limits.

We estimated the value of ν for PC_4-TFSI in both non-ionic DMF and mixtures of DMF with Bmim-TFSI by using the scaling relationship between the specific viscosity η_{sp} and the monomer concentration c_p for SU solutions,[52] given by $\eta_{sp} \propto c_p^{1/(3\nu-1)}$. Applying the scaling of $\eta_{sp} \propto c_p^{0.5}$ observed for the SU solutions of PC_4-TFSI in DMF (see Figure 2b), we obtained $\nu = 1$, in good agreement with the predicted value of $\nu = 1$ for polyelectrolytes in good solvents in the low-salt limit. Similarly, Figure 2b includes the plot of η_{sp} at various c_p for PC_4-TFSI in pure Bmim-TFSI (blue triangles). Here, the values of η_0 were estimated by averaging shear viscosity η values over shear rates in the Newtonian regime (see Figure S9 of the Supporting Information). In Figure 2b, we observed two clear power-law regimes of η_{sp} with respect to c_p for PC_4-TFSI in pure Bmim-TFSI: $\eta_{sp} \propto c_p^{1.0}$ for $c_p < 4.0 \times 10^{-2}$ M in the DL regime, and $\eta_{sp} \propto c_p^{1.3}$ for $4.0 \times 10^{-2}\ M \leq c_p < 0.2$ M in the SU regime. Thus, we obtained the Flory exponent $\nu = 0.59$ for the SU solutions of PC_4-TFSI in Bmim-TFSI, very close to the predicted value of $\nu = 0.6$ for polyelectrolytes in good solvents in the high-salt limit. These results indicate that both non-ionic DMF and pure Bmim-TFSI act as a good solvent for PC_4-TFSI. Because the solvent mixture consists of DMF and Bmim-TFSI, both acting as good solvents for PC_4-TFSI, it is reasonable to assume that our solvent mixtures also serve as good solvents for PC_4-TFSI, further supported by the fact that PC_4-TFSI was dissolved very quickly in the mixture of DMF and Bmim-TFSI.

4.3.1.3. Solvent Dynamics in the Presence of Polymers. In calculating the specific viscosity, we inherently assumed that the solvent contribution to the polymer solution viscosity was given by the solvent viscosity η_s. However, previous dynamic and calorimetric studies reported that the effective solvent viscosity, that is, the solvent contribution to the polymer solution viscosity, was different from the viscosity of the neat solvent.[92−95] Some prior studies also showed that the addition of salts modified the viscosity of ionic liquids.[96−100] These results suggest that the effective solvent viscosity of our solvent mixtures in the PC_4-TFSI solution may be altered by the

https://doi.org/10.1021/acs.macromol.1c00576
Macromolecules 2021, 54, 5648−5661

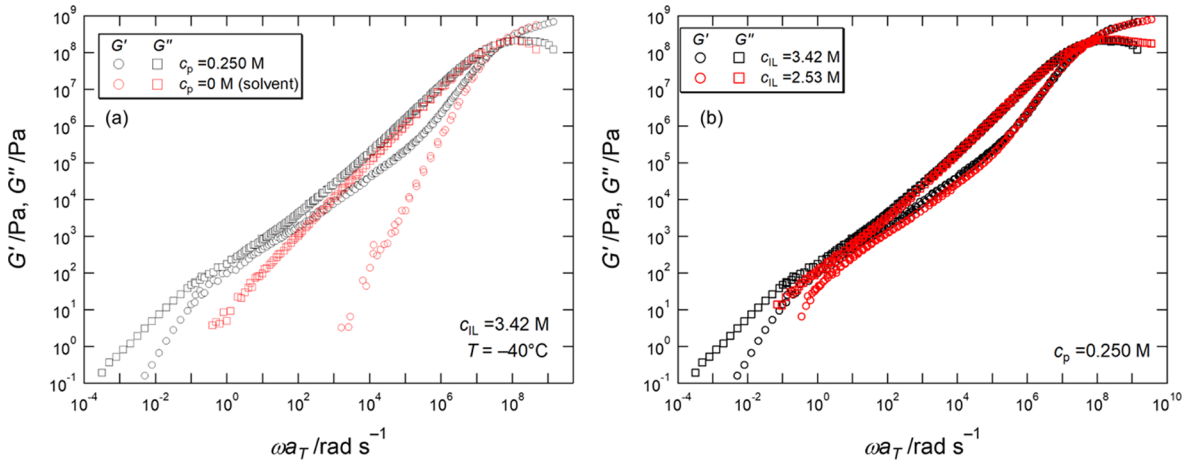

Figure 4. (a) Dynamic storage G' (circles) and loss G'' (squares) moduli as a function of the angular frequency ω for PC_4-TFSI in Bmim-TFSI at c_p = 0.250 M (black symbols) and for the neat Bmim-TFSI (red symbols). The composite curves are constructed by using the reduced variable method with shift factors a_T at a reference temperature T_r = −40 °C. (b) Comparison of the frequency dependence of the complex modulus G^* for two PC_4-TFSI solutions at c_p = 0.250 M with c_{IL} = 3.42 M (black symbols) and c_{IL} = 2.53 M (red symbols).

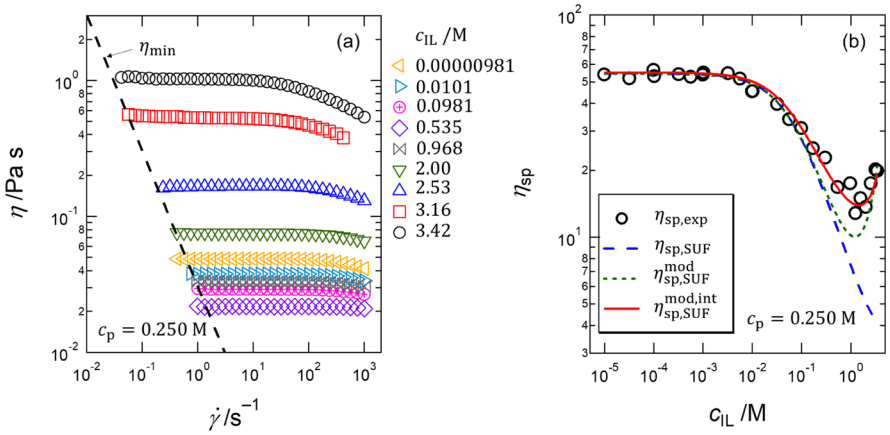

Figure 5. (a) Shear viscosity curves for PC_4-TFSI solutions at c_p = 0.250 M with different Bmim-TFSI concentrations c_{IL} at 25 °C. The dashed line indicates the minimum measurable shear viscosity η_{min}, below which the measured η are removed. (b) Specific viscosity η_{sp} at 25 °C as a function of the Bmim-TFSI concentration c_{IL} for PC_4-TFSI solutions at c_p = 0.250 M. Blue-dashed curve represents the scaling law of $\eta_{sp,SU}$ for SU solutions (eq 4) with A = 2 and $c_{res,tot}$ = $(9.24 \times 10^{-6} + 0.009c_p)$ M, predicted by Dobrynin et al.[20] Green-dotted curve represents the modified scaling law of $\eta^{mod}_{sp,SU}$ for polyelectrolyte SU solutions, given by eq 9 with A = 2, $c_{res,tot}$ = $(9.24 \times 10^{-6} + 0.009c_p)$ M, and a = 0.54 nm. The red solid curve represents the predicted curve of $\eta^{mod,int}_{sp,SU}$, based on our new charge screening model for polyelectrolyte SU solutions, given by eq 11 with A = 2, c_{salt} = $c_{res,tot}$ = $(9.24 \times 10^{-6} + 0.009c_p)$ M, $\eta^{int}_{sp,SU}$ = 6.0, and a = 0.49 nm. The error bars are smaller than the size of symbols and thus omitted.

addition of PC_4-TFSI. Therefore, we examine the effect of the polymer addition on the dynamics of solvent molecules by measuring the complex modulus G^* of PC_4-TFSI solutions as a function of the angular frequency ω. We chose c_{IL} = 3.42 M and c_{IL} = 2.53 M as representative Bmim-TFSI concentrations where their specific viscosity values were different from each other.

Figure 4a compares the dependence of the complex modulus G^* (= G' + iG'') on ω before and after the addition of PC_4-TFSI in pure Bmim-TFSI at c_p = 0.250 M and c_{IL} = 3.42 M. Here, we used the method of reduced variables, the so-called time−temperature superposition principle, to construct the composite curves.[101] The reference temperature was chosen as T_r = −40 °C for both the polymer solution and the neat solvent. The obtained time−temperature shift factors a_T are provided in Figure S10 of the Supporting Information. For ωa_T > 10^7 rad s^{-1}, the dependence of G^* on ω of the neat solvent was close to those of the PC_4-TFSI solution at c_p = 0.250 M. However, as the frequency decreased from 10^7 rad s^{-1} to 10^5 rad s^{-1}, the values of G^* for the PC_4-TFSI solution started to deviate toward low frequencies in comparison to those of the neat solvent. A similar deviation was observed for solutions of polymers with higher glass transition temperatures than those of solvents and accounted for by the increase in local friction due to the cooperative motions of polymer chains and solvent molecules.[93,102] When ωa_T < 10^5 rad s^{-1}, the value of the storage modulus G' was significantly larger than that of the neat solvent, corresponding to the polymer relaxation processes. We observed a similar trend of G^* at c_{IL} = 2.53 M between the PC_4-TFSI solution at c_p = 0.250 M and the neat solvent (see Figure S11 of the Supporting Information). These results indicate that the solvent dynamics of the solvent mixture of DMF and Bmim-TFSI are retarded by the addition of PC_4-TFSI.

When the degree of the retardation of the solvent dynamics by the addition of polymers depends on c_{IL}, the specific viscosity needs to be calculated using the effective solvent viscosity in PC_4-TFSI solutions. We, therefore, compared the

https://doi.org/10.1021/acs.macromol.1c00576
Macromolecules 2021, 54, 5648−5661

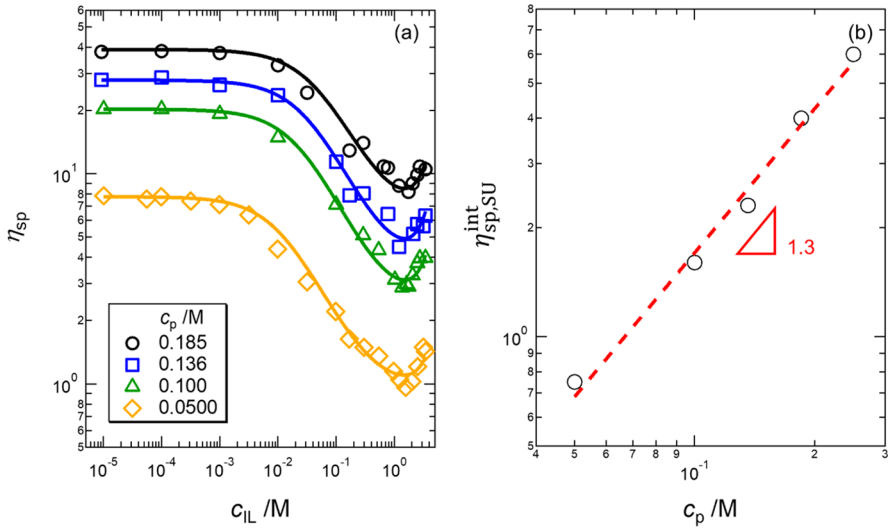

Figure 6. (a) Dependence of the specific viscosity η_{sp} at 25 °C on the Bmim-TFSI concentration c_{IL} for PC_4-TFSI solutions at various monomer concentrations c_p: c_p = 0.185 M (black circles), c_p = 0.136 M (blue squares), c_p = 0.100 M (green triangles), and c_p = 0.0500 M (orange diamonds). Solid curves represent the predicted curve of $\eta^{mod,int}_{sp,SU}$ for SU solutions of polyelectrolytes, given by eq 11 with A = 2, $c_{res,tot}$ = $(9.24 \times 10^{-6} + 0.009c_p)$ M, and a = 0.49 nm at $\eta^{int}_{sp,SU}$=4.0 for c_p = 0.185 M, $\eta^{int}_{sp,SU}$=2.3 for c_p = 0.136 M, $\eta^{int}_{sp,SU}$=1.6 for c_p = 0.100 M, and $\eta^{int}_{sp,SU}$ = 0.75 for c_p = 0.050 M. The obtained values of the scaling prefactor K_1 are provided in Table S1 of the Supporting Information. The error bars are smaller than the size of symbols and thus omitted. (b) Dependence of the intrinsic specific viscosity $\eta^{int}_{sp,SU}$ at 25 °C on the monomer concentration c_p. Red-dashed line represents the power-law fit of $\eta^{int}_{sp,SU}$ with an exponent of 1.3.

frequency dependence of G^* for two PC_4-TFSI solutions at c_{IL} = 3.42 M and c_{IL} = 2.53 M, at a fixed polymer concentration c_p = 0.250 M. In Figure 4b, the G^* data at c_{IL} = 2.53 M were horizontally shifted such that the crossover frequency of G' and G'' at high frequencies matched with that of the G^* at c_{IL} = 3.42 M. For $\omega a_T > 10^6$ rad s^{-1}, the frequency dependence of G^* at c_{IL} = 2.53 M was found to be identical with that at c_{IL} = 3.42 M, indicating an equivalent retardation of the solvent dynamics between these solutions. On the other hand, we observed the difference in G^* for $\omega a_T < 10^{-5}$ rad s^{-1}, suggesting the conformation change of the PC_4-TFSI chains.

Our results demonstrate that the solvent dynamics is retarded by the addition of PC_4-TFSI, but the degree of retardation of the solvent dynamics is independent of c_{IL}. Therefore, we will treat the effective solvent viscosity in the PC_4-TFSI solution as the viscosity of the solvent mixture provided in Figure 3a in the following studies of the viscoelastic properties of PC_4-TFSI in the mixture of DMF and Bmim-TFSI.

4.3.2. Specific Viscosity. We now discuss the charge screening mechanism of PIL (PC_4-TFSI) in IL (Bmim-TFSI) solutions by performing systematic rheological characterizations, varying both IL and PIL concentrations. Figure 5a shows the dependence of the shear viscosity η at 25 °C on shear rate $\dot{\gamma}$ at various representative IL concentrations for PC_4-TFSI solutions with c_p = 0.250 M. At $c_{IL} = 9.81 \times 10^{-6}$ M, η was initially independent of $\dot{\gamma}$ until $\dot{\gamma}^* = 10^2$ s^{-1}, followed by the shear-thinning behavior when $\dot{\gamma} > \dot{\gamma}^*$. The value of η decreased with increasing c_{IL} for c_{IL} < 0.535 M, but started to increase as c_{IL} was further increased. On the other hand, the value of $\dot{\gamma}^*$ increased with increasing c_{IL} at low c_{IL}, but decreased with increasing c_{IL} at high c_{IL}. The observed increase in η is mainly due to the increase in the shear viscosity of the solvent mixture η_s with increasing c_{IL} (see Figure 3a).

In order to eliminate the contribution of the variation in η_s to the solution viscosity, we plotted the specific viscosity η_{sp} as a function of c_{IL} in Figure 5b. The values of η_{sp} were always above one, verifying that our solutions are in the SU regime over the entire c_{IL} range at c_p = 0.250 M. The specific viscosity η_{sp} was initially a constant for $c_{IL} < 3.0 \times 10^{-3}$ M and started to decrease with increasing c_{IL}, exhibiting a typical charge screening behavior predicted by Dobrynin et al. (see eq 4).[20] Interestingly, the value of η_{sp} reached a minimum at $c_{IL} \approx 2$ M, but started to increase when c_{IL} > 2 M.

We compared the dependence of the measured η_{sp} on c_{IL} with Dobrynin's scaling law for SU solutions (eq 4 with A = 2 and $c_{res,tot} = (9.24 \times 10^{-6} + 0.009c_p)$ M), shown as the blue-dashed curve in Figure 5b, displaying good agreement with the measured data for $c_{IL} \leq 0.1$ M. At higher IL concentrations, the measured η_{sp} deviated from Dobrynin's scaling prediction and its value was always larger than predicted with a non-monotonic trend. This observation indicates that the DH theory breaks down at high IL concentrations, similar to the discrepancy between the experimental data and Dobrynin's scaling predictions being reported for PIL solutions in the dilute regime at high IL concentrations.[23]

Next, we fit the measured η_{sp} to our proposed modified scaling law of $\eta^{mod}_{sp,SU}$, given by eq 9 with the modified screening length r^{mod}_B. The best fit was obtained with the ion diameter a = 0.54 nm and shown as the green-dotted curve in Figure 5b. Here, the monomer size b was assumed to be equal to the ion diameter a because the chemical structure of the repeating units of PC_4-TFSI is similar to the chemical structure of Bmim-TFSI. The predicted curve of $\eta^{mod}_{sp,SU}$ captured the dependence of the measured η_{sp} on c_{IL} in the measured c_{IL} range. In particular, the upturn observed at high c_{IL} was explained by our modified scaling law of $\eta^{mod}_{sp,SU}$. However, the measured η_{sp} is still larger than the predicted values of $\eta^{mod}_{sp,SU}$ for SU solutions at c_{IL} > 0.1 M.

The observed small discrepancy between the measured η_{sp} and the modified scaling predication $\eta^{mod}_{sp,SU}$ can be potentially explained by the complete charge screening effect at high IL concentrations. The measured η_{sp} was, therefore, fitted to our new charge screening model of $\eta^{mod,int}_{sp,SU}$ for SU solutions of

https://doi.org/10.1021/acs.macromol.1c00576
Macromolecules 2021, 54, 5648−5661

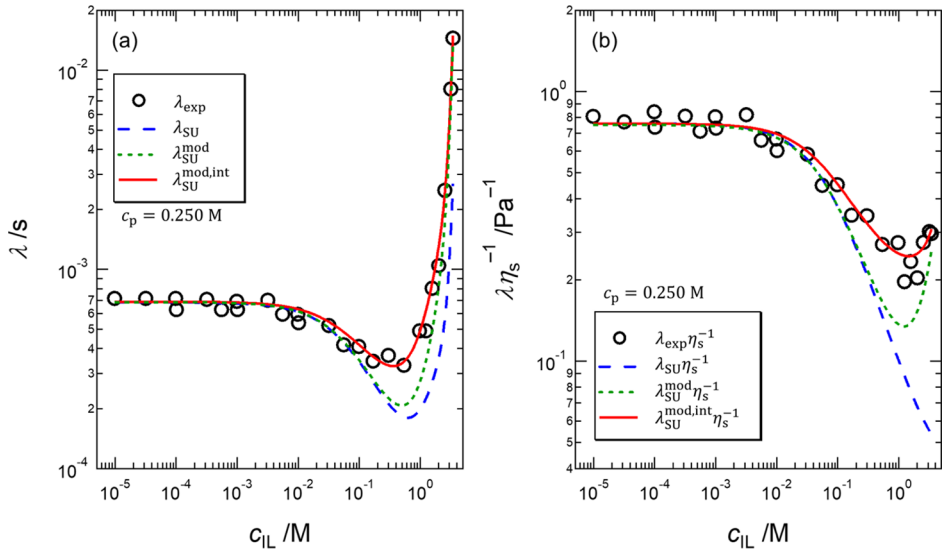

Figure 7. (a) Longest relaxation time λ at 25 °C as a function of the concentration of Bmim-TFSI c_{IL} for PC_4-TFSI solutions at c_p = 0.250 M. (b) Normalized longest relaxation time by the solvent viscosity λ/η_s as a function of c_{IL} at c_p = 0.250 M. In the plot, blue-dashed curve represents the scaling law of λ_{SU} for SU solutions, given by eq 5 with A = 2 and $c_{res,tot}$ = $(9.24 \times 10^{-6} + 0.009c_p)$ M, predicted by Dobrynin et al.[20] The green-dotted curve represents our modified scaling law λ_{SU}^{mod} for polyelectrolyte SU solutions, given by eq 10 with A = 2, $c_{res,tot} = (9.24 \times 10^{-6} + 0.009c_p)$ M, and a = 0.54 nm, while the red solid curve represents our new charge screening model of $\lambda_{SU}^{mod,int}$ for polyelectrolyte SU solutions, given by eq 12 with A = 2, $c_{res,tot}$ = $(9.24 \times 10^{-6} + 0.009c_p)$ M, a = 0.49 nm, and $\lambda_{SU}^{mod,int}\eta_s^{-1}$ = 0.15.

polyelectrolytes, given by eq 11 with r_B^{mod} and the intrinsic specific viscosity $\eta_{sp,SU}^{int}$. The best fit was obtained at a = 0.49 nm and $\eta_{sp,SU}^{int}$ = 6.0, shown as the red solid curve in Figure 5b. The predicted curve of $\eta_{sp,SU}^{mod,int}$ agreed remarkably well with the measured η_{sp} over the measured c_{IL} range covering low to high IL concentration regimes. We tested further the validity of our proposed model of $\eta_{sp,SU}^{mod,int}$ based on eq 11, showing a monotonic decrease of the normalized specific viscosity, $\eta_{sp}^{nor} = (\eta_{sp} - \eta_{sp,SU}^{int})/\left(1 + \frac{a^3}{r_B^3}\right)^{3/2}$, with increasing c_{IL}, consistent with Dobrynin's scaling prediction of $\eta_{sp,SU}$, given by eq 4 (see Section S6 of the Supporting Information for more details). The ion diameter from our curve fit was about 1.2 times larger than the value predicted by Lee et al.[42] This might be explained by considering a three dimensional charge screening process on charged molecules, leading to a larger effective ion diameter due to steric constraints compared to the ion diameter estimated from the screening process on a smooth plate from surface force measurements.[41,42]

When the monomer concentration c_p varied from 0.250 to 0.0500 M, the specific viscosity η_{sp} at a given c_{IL}, shown in Figure 6a, decreased with decreasing c_p. Here, the shear viscosity curves at each c_p used to estimate the zero-shear viscosity η_0 at 25 °C are provided in Figure S12 of the Supporting Information. The decrease in the solution viscosity with decreasing c_p is a reasonable trend because the number of polymer chains decreases with decreasing c_p. More importantly, we found that the dependence of η_{sp} on c_{IL} at a fixed c_p did not change when c_p was decreased. In particular, we observed consistent upturns of η_{sp} at $c_{IL} \approx 2$ M regardless of c_p. These results suggest that the variation of η_{sp} with c_{IL} is caused by the charge screening phenomena by IL ions. We, therefore, compared the measured η_{sp} with our charge screening model $\eta_{sp,SU}^{mod,int}$, given by eq 11, using the ion diameter a = 0.49 nm estimated from the curve fit of η_{sp} at c_p = 0.250 M. Thus, there are only two adjustable parameters in the curve fitting, that is, the scaling prefactor K_1 and the intrinsic specific viscosity $\eta_{sp,SU}^{mod,int}$. Figure 6a includes the best fit curve for η_{sp} at each c_p, showing good agreement with the experimental data at varying c_p in the SU regime. The values of K_1 used in the curve fitting are provided in Table S1 of the Supporting Information.

Using $\eta_{sp,SU}^{int}$ estimated from the curve fitting, we can justify the use of the constant quantity of intrinsic specific viscosity introduced in our charge screening model. If $\eta_{sp,SU}^{int}$ is not an arbitrary constant but related to the size of PC_4-TFSI chain without charges, the value of $\eta_{sp,SU}^{int}$ must increase with increasing c_p and follow the scaling of η_{sp} for neutral polymers in good solvents. Figure 6b shows the dependence of $\eta_{sp,SU}^{int}$ on c_p obtained from the curve fitting of the measured η_{sp} shown in Figures 5b and 6a using $\eta_{sp,SU}^{mod,int}$ in eq 11 at a = 0.49 nm. The value of $\eta_{sp,SU}^{int}$ increased with increasing monomer concentrations and scaled as $\eta_{sp,SU}^{int} \propto c_p^{1.3}$. The obtained power-law exponent agreed well with the predicted exponent of η_{sp} ($\propto c_p^{1.3}$) for neutral polymers in good solvents.[52]

4.3.3. Longest Relaxation Time. The longest relaxation time λ of a viscoelastic liquid is an important rheological parameter because it can be connected to the shear viscosity η through a viscoelastic model, such as the Rouse model. Thus, the measurement of both λ and η allows the verification of the proposed model.

Figure 7a displays the dependence of the longest relaxation time λ on c_{IL} at c_p = 0.250 M. Here, the values of λ at 25 °C were estimated from the dependence of the storage, G', and loss, G'', modulus on angular frequency ω (see more details in Section S7). The longest relaxation time λ was initially a constant for $c_{IL} < 3.0 \times 10^{-3}$ M and decreased with increasing c_{IL} until c_{IL} = 0.6 M. At higher c_{IL}, λ first reached a minimum but increased significantly with increasing c_{IL} by a factor of 10 until c_{IL} reached its saturation value, that is, the salt concentration of pure IL (Bmim-TFSI). The significant increase in λ at high c_{IL} is due predominantly to the increase in the shear viscosity of the solvent mixture η_s at high c_{IL} (see Figure 3a). Based on eqs 5, 10, and 12, λ was therefore normalized by η_s, and its value was plotted as a function of c_{IL}

https://doi.org/10.1021/acs.macromol.1c00576
Macromolecules 2021, 54, 5648−5661

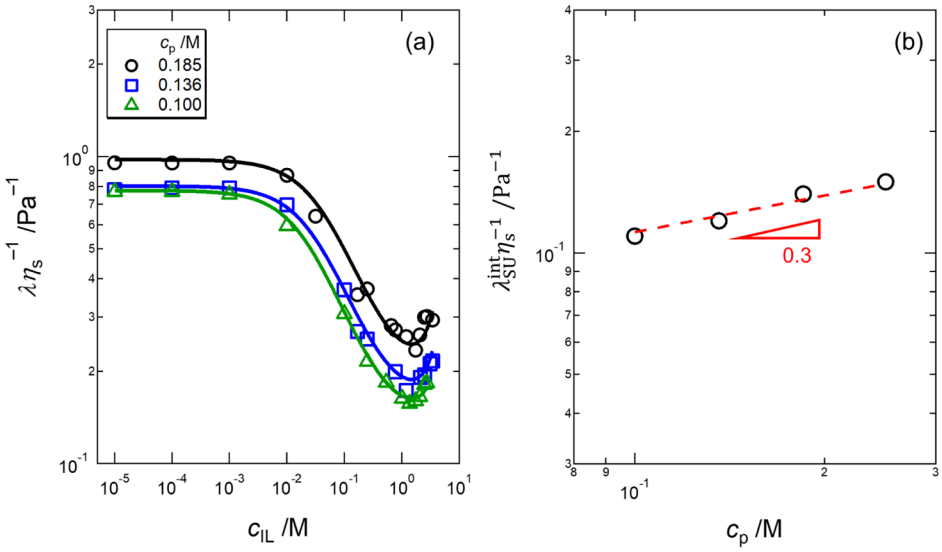

Figure 8. (a) Dependence of the measured λ/η_s at 25 °C on the Bmim-TFSI concentration c_{IL} for the PC_4-TFSI solutions at three different monomer concentrations c_p: c_p = 0.185 M (black circles), c_p = 0.136 M (blue squares), and c_p = 0.100 M (green triangles). Solid curves represent the best fit of the measured λ/η_s to the proposed charge screening model of $\eta_{sp,SU}^{mod,int}$ for polyelectrolyte SU solutions, given by eq 12 at a = 0.49 nm with the varying intrinsic longest relaxation time λ_{SU}^{int}. (b) Value of $\lambda_{SU}^{int}/\eta_s$ is plotted as a function of the monomer concentration c_p. Red-dashed line represents the power-law fit of the measured $\lambda_{SU}^{int}/\eta_s$ with a power-law exponent of 0.3. The values of the scaling prefactor K_2 obtained from the curve fitting are provided in Table S1 of the Supporting Information.

in Figure 7b. The value of λ/η_s remained as a constant for $c_{IL} < 3.0 \times 10^{-3}$ M, and decreased with increasing c_{IL} until $c_{IL} \approx 2$ M, similar to the trend of λ versus c_{IL}. On the other hand, the value of λ/η_s started to increase with increasing c_{IL}, similar to the trend of η_{sp} versus c_{IL} as shown in Figure 5b.

We compared the dependence of the measured λ on c_{IL} with Dobrynin's scaling law of λ_{SU} for SU solutions in the low-salt concentration regime, given by eq 5. The predicted curve (blue-dashed curve) of λ_{SU} with A = 2 and $c_{res,tot} = (9.24 \times 10^{-6} + 0.009c_p)$ M agreed well with the experimental data for $c_{IL} \leq 0.05$ M, but the measured λ for $c_{IL} > 0.05$ M was always larger than predicted. In the curve fitting, we used eq 13 to predict the value of η_s of the solvent mixture. The deviation from Dobrynin's scaling prediction was also observed in the plot of λ/η_s versus c_{IL}, shown in Figure 7b. In this case, while Dobrynin's scaling law predicted a monotonic decrease of λ/η_s with the increasing IL concentration, the experimental data showed an upturn at $c_{IL} \approx 2$ M, similar to the behavior of the measured η_{sp} (see Figure 5b). Therefore, we fitted the measured λ with the modified scaling law of λ_{SU}^{mod} for polyelectrolyte SU solutions accounting only for the modified screening length, given by eq 10 using the value a = 0.54 nm obtained from the previous curve fitting of η_{sp}. The predicted curves of λ_{SU}^{mod} and $\lambda_{SU}^{mod}/\eta_s$ (shown as the green-dotted curve in Figure 7a,b) captured the dependence of both λ and λ/η_s on c_{IL}, but the measured λ is still larger than λ_{SU}^{mod} for $c_{IL} > 0.1$ M, similar to the observation on the comparison between the measured η_{sp} and the scaling prediction of $\eta_{sp,SU}^{mod}$ (see Figure 5b). Subsequently, we compared the measured λ with the proposed charge screening model of $\lambda_{SU}^{mod,int}$, and the best fit of both λ and λ/η_s (red solid curve in Figures 7a,b) was obtained using eq 12 with a = 0.49 nm and $\lambda_{SU}^{int}/\eta_s$ = 0.15 Pa^{-1}. The predicted curve of $\lambda_{SU}^{mod,int}/\eta_s$ described well the dependence of both λ and λ/η_s on c_{IL} over the measured c_{IL} range. We emphasize that the estimated ion diameter a = 0.49 nm is identical with that obtained from the curve fitting of the measured η_{sp} with $\eta_{sp,SU}^{mod,int}$.

Similar to the discussion on the intrinsic specific viscosity $\eta_{sp,SU}^{int}$, if $\lambda_{SU}^{mod,int}$ reflects the initial size of the PC_4-TFSI chain, the scaling of $\lambda_{SU}^{mod,int}$ with respect to c_p must follow the scaling of λ predicted for electrically neutral polymers in good solvents. Figure 8a shows the dependence of λ/η_s on c_{IL} for PC_4-TFSI solutions at different c_p in the SU regime. The value of λ at low c_{IL} increased slightly with increasing c_p, which disagrees with Dobrynin's scaling prediction of λ ($\propto c_p^{-1/2}$). Considering the observed deviation of the measured η_{sp} from Dobrynin's scaling prediction of $\eta_{sp,SU}$ at high c_p in the SU regime (see Figure 2b), this discrepancy might be caused by the complexity of the scaling for solutions where both electrostatic and polydispersity effects coexist. Nevertheless, the dependence of λ/η_s on c_{IL} was independent of the monomer concentration c_p, suggesting that the variation of λ/η_s with c_{IL} occurs due to the charge screening by IL ions. We, therefore, compared the measured λ/η_s with $\lambda_{SU}^{mod,int}/\eta_s$ in eq 12, proposed by our charge screening model. Again, we applied the ion diameter a = 0.49 nm obtained from the curve fitting of λ/η_s for the solution at c_p = 0.250 M. The best fits are provided as solid curves in Figure 8a and showed good agreement with the experimental results for all the tested solutions. The obtained value of $\lambda_{SU}^{int}/\eta_s$ for each c_p is then plotted as a function of c_p in Figure 8b. We found that $\lambda_{SU}^{int}/\eta_s$ increased with increasing c_p and was scaled as $\lambda_{SU}^{int}/\eta_s \propto c_p^{0.3}$, in good agreement with the predicted scaling of $\lambda \propto c_p^{0.31}$ for neutral polymers in good solvents.[52] The values of K_2 obtained from the curve fitting are provided in Table S1 of the Supporting Information.

4.4. Electrostatic Length Scales for PC_4-TFSI in IL Solutions. Comparison among different electrostatic length scales allows quantitative argument on which charge screening mechanism operates in a given IL concentration regime. We computed three electrostatic length scales: the Bjerrum length l_B, the screening length r_B, and the modified screening length r_B^{mod} for PC_4-TFSI in the mixture of DMF and Bmim-TFSI, based on Dobrynin's and our modified charge screening

https://doi.org/10.1021/acs.macromol.1c00576
Macromolecules 2021, 54, 5648−5661

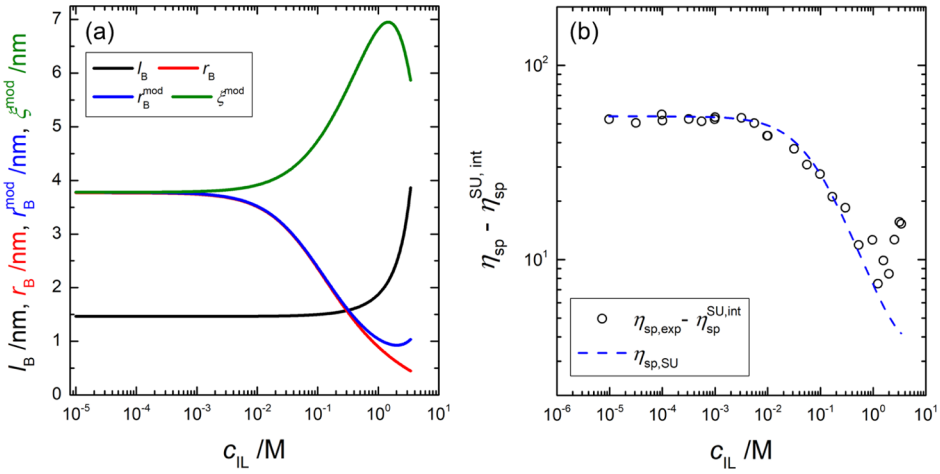

Figure 9. (a) Dependence of the Bjerrum length l_B, Dobrynin's screening length r_B (eq 2), the modified screening length r_B^{mod} (eq 7), and the modified correlation length ξ^{mod} (eq 8) on the IL concentration c_{IL} at 25 °C. The values of r_B, r_B^{mod}, and ξ^{mod} are computed with $A = 2$, $c_p = 0.25$ M, $a = 0.49$ nm, and $c_{res,tot} = (9.24 \times 10^{-6} + 0.009c_p)$ M. (b) Measured specific viscosity $\eta_{sp,exp}$ at $c_p = 0.25$ M subtracted by the intrinsic specific viscosity $\eta_{sp,SU}^{int} = 6.0$, that is, $(\eta_{sp} - \eta_{sp,SU}^{int})$, is compared with Dobrynin's scaling prediction of $\eta_{sp,SU}$, given by eq 4.

models. The values of l_B, r_B, and r_B^{mod} at $T = 25$ °C were calculated using $c_p = 0.25$ M, $a = 0.49$ nm, and $c_{res,tot} = (9.24 \times 10^{-6} + 0.009c_p)$ M, and plotted as a function of the Bmim-TFSI concentration c_{IL}, see Figure 9a. The Bjerrum length l_B increases with increasing c_{IL} due to a monotonic decrease in the dielectric constant of the solvent mixture of DMF and Bmim-TFSI, shown in Figure 3b. On the other hand, the screening length r_B decreases monotonically with increasing c_{IL}, as predicted by the DH theory. The crossover of l_B and r_B is observed at $c_{IL} \approx 0.3$ M, suggesting the breakdown of the DH theory for $c_{IL} > 0.3$ M because the DH theory assumes $l_B \ll r_B$.[42] Consistently, the measured η_{sp} after subtracting the intrinsic specific viscosity $\eta_{sp,SU}^{int}$, that is, $(\eta_{sp} - \eta_{sp,SU}^{int})$, becomes larger than Dobrynin's scaling prediction value for $c_{IL} > 0.3$ M, as shown in Figure 9b. Note that subtraction of $\eta_{sp,SU}^{int}$ is necessary because the measured η_{sp} values are influenced by both electrostatic interaction and the complete charge screening effects, while Dobrynin's scaling prediction of η_{sp} accounts only for the electrostatic effect.

Above the crossover ion concentration, ion−ion interactions are expected to play a significant role in the charge screening mechanism in IL solutions. Lee et al.[42] proposed that strong ionic correlation would modify electrostatic behavior in IL solutions, and the charge screening is characterized by a modified screening length r_B^{mod}. In particular, the strong ionic correlation effect was predicted to become dominant when r_B approaches the salt ion diameter a. We observed $r_B \approx a$ (= 0.49 nm) at $c_{IL} \approx 2$ M, at which an upturn in r_B^{mod} is also displayed with increasing c_{IL}. Consistently, an upturn of the measured $(\eta_{sp} - \eta_{sp,SU}^{int})$ is observed at $c_{IL} \approx 2$ M, as seen in Figure 9b. Figure 9 clearly demonstrates that the Debye screening mechanism operates at low c_{IL}, while strong ion correlation dominates the charge screening behavior at high c_{IL}.

In summary, we have demonstrated that the charge screening effect on the viscoelastic properties of PILs in IL solutions can be quantitatively explained by using our new charge screening model, which accounts for both the modified screening length and complete charge screening at high IL concentrations. Our charge screening model suggests that the correlation length of PC_4-TFSI chains increases initially with the increasing IL concentration at low IL concentrations, but reaches a maximum and then decreases as the IL concentrations are further increased. According to eq 8, the observed behavior at high IL concentrations will be enhanced as the ion diameter increases. On the other hand, when the ion diameter of salts is sufficiently small, such as sodium chloride, our model predicts either a monotonic decrease or an asymptotic behavior of properties with the increasing IL concentrations, depending on the flexibility of polyelectrolyte backbones. Such a behavior has been experimentally observed in many ordinary polyelectrolyte solutions containing small salts.[27,75,77,78,80,84,85,103,104] These interesting features warrant more in-depth studies in the future.

5. CONCLUSIONS

In this work, we investigated the effect of the electrostatic screening on the viscoelastic properties of PILs in IL solutions in the SU polymer regime by measuring the specific viscosity η_{sp} and the longest relaxation time λ of a PIL, PC_4-TFSI, in a mixture of a non-ionic solvent, DMF, and an ionic liquid, Bmim-TFSI. We observed that both η_{sp} and λ were initially a constant at low c_{IL} and started to decrease with increasing c_{IL} at intermediate c_{IL}. At sufficiently high c_{IL}, the values of η_{sp} and λ reached a minimum and then increased with increasing c_{IL}. Comparing the measured trend of η_{sp} and λ versus c_{IL} with the scaling laws by Dobrynin et al.,[20] we found good agreement in the low IL concentration regime, beyond which there was a significant deviation between the experimental data and the existing scaling predictions. We propose a new charge screening model by revising the scaling law accounting for both the modified screening length in concentrated salt solutions and the complete charge screening. This new model captured the measured η_{sp} and λ values remarkably well over the entire IL concentration range. These results suggest that the correlation length of polymer chains increases initially with increasing c_{IL} due to the charge screening effect, but reaches a maximum, followed by a downturn due to strong ionic correlations at high IL concentrations. Our studies demonstrate how the strong ionic correlation modifies the electrostatics of PILs in the presence of moderate polymer−polymer interactions, thus providing good strategies for the

https://doi.org/10.1021/acs.macromol.1c00576
Macromolecules 2021, 54, 5648−5661

material design of PIL solutions to improve polymer-processing operations.

■ ASSOCIATED CONTENT

Supporting Information

The Supporting Information is available free of charge at https://pubs.acs.org/doi/10.1021/acs.macromol.1c00576.

Comparison between the literature data and Dobrynin's scaling prediction; residual salt concentration; high-frequency shear rheology via diffusing wave spectroscopy; charge screening model for dilute polyelectrolyte solutions from low to high salt concentrations; estimation of the dielectric constant for the solvent mixture of DMF and Bmim-TFSI; verification of the proposed charge screening model: normalization of the specific viscosity; estimation of the longest relaxation time; density ρ of the solvent mixture of DMF and Bmim-TFSI; shear viscosity curves for PC_4-TFSI in pure Bmim-TFSI with various monomer concentrations; temperature dependence of shift factors a_T; comparison of the complex modulus G^* between PC_4-TFSI in the mixture of DMF and Bmim-TFSI at c_p = 0.250 M and c_{IL} = 2.53 M and the neat solvent at c_p = 0 M and c_{IL} = 2.53 M; shear viscosity curves for PC_4-TFSI solutions at various c_p; and scaling prefactors used in the curve fitting (PDF)

■ AUTHOR INFORMATION

Corresponding Authors

Atsushi Matsumoto − *Micro/Bio/Nanofluidics Unit, Okinawa Institute of Science and Technology Graduate University, Okinawa 904-0495, Japan; Department of Applied Chemistry and Biotechnology, University of Fukui, Fukui 910-8507, Japan;* orcid.org/0000-0002-8157-3083; Email: atsushi5@u-fukui.ac.jp

Amy Q. Shen − *Micro/Bio/Nanofluidics Unit, Okinawa Institute of Science and Technology Graduate University, Okinawa 904-0495, Japan;* orcid.org/0000-0002-1222-6264; Email: amy.shen@oist.jp

Authors

Ryota Yoshizawa − *Department of Macromolecular Science, Osaka University, Toyonaka, Osaka 560-0043, Japan*

Osamu Urakawa − *Department of Macromolecular Science, Osaka University, Toyonaka, Osaka 560-0043, Japan;* orcid.org/0000-0001-5071-208X

Tadashi Inoue − *Department of Macromolecular Science, Osaka University, Toyonaka, Osaka 560-0043, Japan;* orcid.org/0000-0002-9934-1299

Complete contact information is available at: https://pubs.acs.org/10.1021/acs.macromol.1c00576

Notes

The authors declare no competing financial interest.

■ ACKNOWLEDGMENTS

The authors acknowledge the support of the Okinawa Institute of Science and Technology Graduate University with subsidy funding from the Cabinet Office, Government of Japan. A.M. acknowledges funding from the Japanese Society for the Promotion of Science (Grants-in-Aid for Early-Career Scientists, grant no. 19K15641). A.Q.S. acknowledges funding from the Japanese Society for the Promotion of Science (Grants-in-Aid for Scientific Research (B), grant no. 18H01135) and the Joint Research Projects (JRPs) supported by JSPS and SNSF. A.M. also acknowledges the support of the University of Fukui to accomplish the present work. The authors thank Dr. Yoshiteru Iinuma from OIST for his help with the use of the inductively coupled plasma mass spectrometer as well as the ion chromatography.

■ REFERENCES

(1) Hayes, R.; Warr, G. G.; Atkin, R. Structure and Nanostructure in Ionic Liquids. *Chem. Rev.* **2015**, *115*, 6357−6426.

(2) Ohno, H.; Ito, K. Room-Temperature Molten Salt Polymers as a Matrix for Fast Ion Conduction. *Chem. Lett.* **1998**, *27*, 751−752.

(3) Matsumoto, A.; Iacob, C.; Noda, T.; Urakawa, O.; Runt, J.; Inoue, T. Introducing Large Counteranions Enhances the Elastic Modulus of Imidazolium-Based Polymerized Ionic Liquids. *Macromolecules* **2018**, *51*, 4129−4142.

(4) Kuray, P.; Noda, T.; Matsumoto, A.; Iacob, C.; Inoue, T.; Hickner, M. A.; Runt, J. Ion Transport in Pendant and Backbone Polymerized Ionic Liquids. *Macromolecules* **2019**, *52*, 6438−6448.

(5) Choi, U. H.; Mittal, A.; Price, T. L.; Lee, M.; Gibson, H. W.; Runt, J.; Colby, R. H. Molecular Volume Effects on the Dynamics of Polymerized Ionic Liquids and their Monomers. *Electrochim. Acta* **2015**, *175*, 55−61.

(6) Plechkova, N. V.; Seddon, K. R. Applications of ionic liquids in the chemical industry. *Chem. Soc. Rev.* **2008**, *37*, 123−150.

(7) Huang, T.; Long, M.-C.; Wang, X.-L.; Wu, G.; Wang, Y.-Z. One-step preparation of poly(ionic liquid)-based flexible electrolytes by in-situ polymerization for dendrite-free lithium ion batteries. *Chem. Eng. J.* **2019**, *375*, 122062.

(8) Choi, U. H.; Price, T. L.; Schoonover, D. V.; Gibson, H. W.; Colby, R. H. The Effect of Oligo(oxyethylene) Moieties on Ion Conduction and Dielectric Properties of Norbornene-Based Imidazolium Tf_2N Ionic Liquid Monomers. *Macromolecules* **2020**, *53*, 4990−5000.

(9) Tang, J.; Sun, W.; Tang, H.; Radosz, M.; Shen, Y. Enhanced CO_2 Absorption of Poly(ionic liquid)s. *Macromolecules* **2005**, *38*, 2037−2039.

(10) Charan, K. T. P.; Pothanagandhi, N.; Vijayakrishna, K.; Sivaramakrishna, A.; Mecerreyes, D.; Sreedhar, B. Poly(ionic liquids) as "smart" stabilizers for metal nanoparticles. *Eur. Polym. J.* **2014**, *60*, 114−122.

(11) Wu, J.; Mu, L.; Feng, X.; Lu, X.; Larsson, R.; Shi, Y. Poly(alkylimidazolium bis(trifluoromethylsulfonyl)imide)-Based Polymerized Ionic Liquids: A Potential High-Performance Lubricating Grease. *Adv. Mater. Interfaces* **2019**, *6*, 1801796.

(12) Mogurampelly, S.; Ganesan, V. Ion Transport in Polymerized Ionic Liquid-Ionic Liquid Blends. *Macromolecules* **2018**, *51*, 9471−9483.

(13) Chen, H.; Elabd, Y. A. Polymerized Ionic Liquids: Solution Properties and Electrospinning. *Macromolecules* **2009**, *42*, 3368−3373.

(14) Susan, M. A. B. H.; Kaneko, T.; Noda, A.; Watanabe, M. Ion Gels Prepared by in Situ Radical Polymerization of Vinyl Monomers in an Ionic Liquid and Their Characterization as Polymer Electrolytes. *J. Am. Chem. Soc.* **2005**, *127*, 4976−4983.

(15) Zhou, D.; Liu, R.; Zhang, J.; Qi, X.; He, Y.-B.; Li, B.; Yang, Q.-H.; Hu, Y.-S.; Kang, F. In situ synthesis of hierarchical poly(ionic liquid)-based solid electrolytes for high-safety lithium-ion and sodium-ion batteries. *Nano Energy* **2017**, *33*, 45−54.

(16) Forsyth, M.; Porcarelli, L.; Wang, X.; Goujon, N.; Mecerreyes, D. Innovative Electrolytes Based on Ionic Liquids and Polymers for Next-Generation Solid-State Batteries. *Acc. Chem. Res.* **2019**, *52*, 686−694.

(17) Josef, E.; Guterman, R. Designing Solutions for Electrospinning of Poly(ionic liquid)s. *Macromolecules* **2019**, *52*, 5223−5230.

(18) Chen, Q.; Bao, N.; Wang, J.-H. H.; Tunic, T.; Liang, S.; Colby, R. H. Linear Viscoelasticity and Dielectric Spectroscopy of Ionomer/

Plasticizer Mixtures: A Transition from Ionomer to Polyelectrolyte. *Macromolecules* **2015**, *48*, 8240−8252.
(19) Zhang, Z.; Chen, Q.; Colby, R. H. Dynamics of associative polymers. *Soft Matter* **2018**, *14*, 2961−2977.
(20) Dobrynin, A. V.; Colby, R. H.; Rubinstein, M. Scaling Theory of Polyelectrolyte Solutions. *Macromolecules* **1995**, *28*, 1859−1871.
(21) Chen, G.; Perazzo, A.; Stone, H. A. Influence of Salt on the Viscosity of Polyelectrolyte Solutions. *Phys. Rev. Lett.* **2020**, *124*, 177801.
(22) Colby, R. H. Structure and linear viscoelasticity of flexible polymer solutions: comparison of polyelectrolyte and neutral polymer solutions. *Rheol. Acta* **2010**, *49*, 425−442.
(23) Matsumoto, A.; Del Giudice, F.; Rotrattanadumrong, R.; Shen, A. Q. Rheological Scaling of Ionic-Liquid-Based Polyelectrolytes in Ionic Liquid Solutions. *Macromolecules* **2019**, *52*, 2759−2771.
(24) Tudryn, G. J.; Liu, W.; Wang, S.-W.; Colby, R. H. Counterion Dynamics in Polyester−Sulfonate Ionomers with Ionic Liquid Counterions. *Macromolecules* **2011**, *44*, 3572−3582.
(25) Colby, R. H.; Zheng, X.; Rafailovich, M. H.; Sokolov, J.; Peiffer, D. G.; Schwarz, S. A.; Strzhemechny, Y.; Nguyen, D. Dynamics of Lightly Sulfonated Polystyrene Ionomers. *Phys. Rev. Lett.* **1998**, *81*, 3876−3879.
(26) Chen, Q.; Tudryn, G. J.; Colby, R. H. Ionomer dynamics and the sticky Rouse model. *J. Rheol.* **2013**, *57*, 1441−1462.
(27) Lopez, C. G.; Colby, R. H.; Graham, P.; Cabral, J. T. Viscosity and Scaling of Semiflexible Polyelectrolyte NaCMC in Aqueous Salt Solutions. *Macromolecules* **2017**, *50*, 332−338.
(28) Boris, D. C.; Colby, R. H. Rheology of Sulfonated Polystyrene Solutions. *Macromolecules* **1998**, *31*, 5746−5755.
(29) Dou, S.; Colby, R. H. Solution Rheology of a Strongly Charged Polyelectrolyte in Good Solvent. *Macromolecules* **2008**, *41*, 6505−6510.
(30) Lopez, C. G. Scaling and Entanglement Properties of Neutral and Sulfonated Polystyrene. *Macromolecules* **2019**, *52*, 9409−9415.
(31) Takahashi, Y.; Hase, H.; Yamaguchi, M.; Noda, I. Viscoelastic properties of polyelectrolyte solutions. III. Dynamic moduli from terminal to plateau regions. *J. Non-Cryst. Solids* **1994**, *172−174*, 911−916.
(32) Lopez, C. G. Entanglement of semiflexible polyelectrolytes: Crossover concentrations and entanglement density of sodium carboxymethyl cellulose. *J. Rheol.* **2020**, *64*, 191−204.
(33) Akkaoui, K.; Yang, M.; Digby, Z. A.; Schlenoff, J. B. Ultraviscosity in Entangled Polyelectrolyte Complexes and Coacervates. *Macromolecules* **2020**, *53*, 4234−4246.
(34) Kujawa, P.; Audibert-Hayet, A.; Selb, J.; Candau, F. Effect of Ionic Strength on the Rheological Properties of Multisticker Associative Polyelectrolytes. *Macromolecules* **2006**, *39*, 384−392.
(35) Konop, A. J.; Colby, R. H. Polyelectrolyte Charge Effects on Solution Viscosity of Poly(acrylic acid). *Macromolecules* **1999**, *32*, 2803−2805.
(36) Di Cola, E.; Waigh, T. A.; Colby, R. H. Dynamic light scattering and rheology studies of aqueous solutions of amphiphilic sodium maleate containing copolymers. *J. Polym. Sci., Part B: Polym. Phys.* **2007**, *45*, 774−785.
(37) Krause, W. E.; Tan, J. S.; Colby, R. H. Semidilute solution rheology of polyelectrolytes with no added salt. *J. Polym. Sci., Part B: Polym. Phys.* **1999**, *37*, 3429−3437.
(38) Gebbie, M. A.; Valtiner, M.; Banquy, X.; Fox, E. T.; Henderson, W. A.; Israelachvili, J. N. Ionic liquids behave as dilute electrolyte solutions. *Proc. Natl. Acad. Sci. U.S.A.* **2013**, *110*, 9674−9679.
(39) Gebbie, M. A.; Dobbs, H. A.; Valtiner, M.; Israelachvili, J. N. Long-range electrostatic screening in ionic liquids. *Proc. Natl. Acad. Sci. U.S.A.* **2015**, *112*, 7432−7437.
(40) Gebbie, M. A.; Smith, A. M.; Dobbs, H. A.; Lee, A. A.; Warr, G. G.; Banquy, X.; Valtiner, M.; Rutland, M. W.; Israelachvili, J. N.; Perkin, S.; Atkin, R. Long range electrostatic forces in ionic liquids. *Chem. Commun.* **2017**, *53*, 1214−1224.
(41) Smith, A. M.; Lee, A. A.; Perkin, S. The Electrostatic Screening Length in Concentrated Electrolytes Increases with Concentration. *J. Phys. Chem. Lett.* **2016**, *7*, 2157−2163.
(42) Lee, A. A.; Perez-Martinez, C. S.; Smith, A. M.; Perkin, S. Scaling Analysis of the Screening Length in Concentrated Electrolytes. *Phys. Rev. Lett.* **2017**, *119*, 026002.
(43) Gaddam, P.; Ducker, W. Electrostatic Screening Length in Concentrated Salt Solutions. *Langmuir* **2019**, *35*, 5719−5727.
(44) Funari, R.; Matsumoto, A.; de Bruyn, J. R.; Shen, A. Q. Rheology of the Electric Double Layer in Electrolyte Solutions. *Anal. Chem.* **2020**, *92*, 8244−8253.
(45) Gavish, N.; Elad, D.; Yochelis, A. From Solvent-Free to Dilute Electrolytes: Essential Components for a Continuum Theory. *J. Phys. Chem. Lett.* **2018**, *9*, 36−42.
(46) Lee, A. A.; Perez-Martinez, C. S.; Smith, A. M.; Perkin, S. Underscreening in concentrated electrolytes. *Faraday Discuss.* **2017**, *199*, 239−259.
(47) Rotenberg, B.; Bernard, O.; Hansen, J.-P. Underscreening in ionic liquids: a first principles analysis. *J. Phys.: Condens. Matter* **2018**, *30*, 054005.
(48) Coles, S. W.; Park, C.; Nikam, R.; Kanduč, M.; Dzubiella, J.; Rotenberg, B. Correlation Length in Concentrated Electrolytes: Insights from All-Atom Molecular Dynamics Simulations. *J. Phys. Chem. B* **2020**, *124*, 1778−1786.
(49) Adar, R. M.; Safran, S. A.; Diamant, H.; Andelman, D. Screening length for finite-size ions in concentrated electrolytes. *Phys. Rev. E* **2019**, *100*, 042615.
(50) Cats, P.; Evans, R.; Härtel, A.; van Roij, R. Primitive model electrolytes in the near and far field: Decay lengths from DFT and simulations. *J. Chem. Phys.* **2021**, *154*, 124504.
(51) Anousheh, N.; Solis, F. J.; Jadhao, V. Ionic structure and decay length in highly concentrated confined electrolytes. *AIP Adv.* **2020**, *10*, 125312.
(52) Rubinstein, M.; Colby, R. H. *Polymer Physics*; Oxford University Press: New York, 2003.
(53) Marcilla, R.; Blazquez, J. A.; Fernandez, R.; Grande, H.; Pomposo, J. A.; Mecerreyes, D. Synthesis of Novel Polycations Using the Chemistry of Ionic Liquids. *Macromol. Chem. Phys.* **2005**, *206*, 299−304.
(54) Macosko, C. W. *Rheology: Principles, Measurements, and Applications*; Wiley-VCH: New York, 1994.
(55) De Gennes, P. G.; Pincus, P.; Velasco, R. M.; Brochard, F. Remarks on polyelectrolyte conformation. *J. Phys.* **1976**, *37*, 1461−1473.
(56) Khokhlov, A. R. On the collapse of weakly charged polyelectrolytes. *J. Phys. A: Math. Gen.* **1980**, *13*, 979−987.
(57) Schiessel, H. Counterion Condensation on Flexible Polyelectrolytes: Dependence on Ionic Strength and Chain Concentration. *Macromolecules* **1999**, *32*, 5673−5680.
(58) Schiessel, H.; Pincus, P. Counterion-Condensation-Induced Collapse of Highly Charged Polyelectrolytes. *Macromolecules* **1998**, *31*, 7953−7959.
(59) Turkoz, E.; Perazzo, A.; Arnold, C. B.; Stone, H. A. Salt type and concentration affect the viscoelasticity of polyelectrolyte solutions. *Appl. Phys. Lett.* **2018**, *112*, 203701.
(60) Dou, S.; Colby, R. H. Charge density effects in salt-free polyelectrolyte solution rheology. *J. Polym. Sci., Part B: Polym. Phys.* **2006**, *44*, 2001−2013.
(61) Del Giudice, F.; Calcagno, V.; Esposito Taliento, V.; Greco, F.; Netti, P. A.; Maffettone, P. L. Relaxation time of polyelectrolyte solutions: When μ-rheometry steps in charge. *J. Rheol.* **2017**, *61*, 13−21.
(62) Lopez, C. G.; Richtering, W. Viscosity of Semidilute and Concentrated Nonentangled Flexible Polyelectrolytes in Salt-Free Solution. *J. Phys. Chem. B* **2019**, *123*, 5626−5634.
(63) Graessley, W. Polymer chain dimensions and the dependence of viscoelastic properties on concentration, molecular weight and solvent power. *Polymer* **1980**, *21*, 258−262.

https://doi.org/10.1021/acs.macromol.1c00576
Macromolecules 2021, 54, 5648−5661

(64) Lopez, C. G.; Rogers, S. E.; Colby, R. H.; Graham, P.; Cabral, J. T. Structure of sodium carboxymethyl cellulose aqueous solutions: A SANS and rheology study. *J. Polym. Sci., Part B: Polym. Phys.* **2015**, *53*, 492−501.
(65) Dubrovskii, S. A.; Zelenetskii, A. N.; Uspenskii, S. A.; Khabarov, V. N. Effect of borax additives on the rheological properties of sodium hyaluronate aqueous solutions. *Polym. Sci., Ser. A* **2014**, *56*, 205−210.
(66) Jimenez, L. N.; Dinic, J.; Parsi, N.; Sharma, V. Extensional Relaxation Time, Pinch-Off Dynamics, and Printability of Semidilute Polyelectrolyte Solutions. *Macromolecules* **2018**, *51*, 5191−5208.
(67) Pabon, M.; Selb, J.; Candau, F. Dynamics of a High Molecular Weight Polyelectrolyte. *Langmuir* **1998**, *14*, 735−737.
(68) Wyatt, N. B.; Gunther, C. M.; Liberatore, M. W. Increasing viscosity in entangled polyelectrolyte solutions by the addition of salt. *Polymer* **2011**, *52*, 2437−2444.
(69) McKee, M. G.; Hunley, M. T.; Layman, J. M.; Long, T. E. Solution Rheological Behavior and Electrospinning of Cationic Polyelectrolytes. *Macromolecules* **2006**, *39*, 575−583.
(70) Oelschlaeger, C.; Cota Pinto Coelho, M.; Willenbacher, N. Chain Flexibility and Dynamics of Polysaccharide Hyaluronan in Entangled Solutions: A High Frequency Rheology and Diffusing Wave Spectroscopy Study. *Biomacromolecules* **2013**, *14*, 3689−3696.
(71) Potier, M.; Tea, L.; Benyahia, L.; Nicolai, T.; Renou, F. Viscosity of Aqueous Polysaccharide Solutions and Selected Homogeneous Binary Mixtures. *Macromolecules* **2020**, *53*, 10514−10525.
(72) Ye, Y.; Yonggang, S.; Zheng, Q. Rheological behavior and molecular relaxation of polycations with macrocounterions in aqueous solutions. *Polym. Chem.* **2016**, *7*, 89−100.
(73) Cho, J.; Heuzey, M.-C.; Bégin, A.; Carreau, P. J. Viscoelastic properties of chitosan solutions: Effect of concentration and ionic strength. *J. Food Eng.* **2006**, *74*, 500−515.
(74) Xu, X.; Liu, W.; Zhang, L. Rheological behavior of Aeromonas gum in aqueous solutions. *Food Hydrocolloids* **2006**, *20*, 723−729.
(75) Sedlák, M. The ionic strength dependence of the structure and dynamics of polyelectrolyte solutions as seen by light scattering: The slow mode dilemma. *J. Chem. Phys.* **1996**, *105*, 10123−10133.
(76) Sedlák, M. What Can Be Seen by Static and Dynamic Light Scattering in Polyelectrolyte Solutions and Mixtures?†. *Langmuir* **1999**, *15*, 4045−4051.
(77) Adamczyk, Z.; Jamroży, K.; Batys, P.; Michna, A. Influence of ionic strength on poly(diallyldimethylammonium chloride) macromolecule conformations in electrolyte solutions. *J. Colloid Interface Sci.* **2014**, *435*, 182−190.
(78) Brunchi, C.-E.; Morariu, S.; Bercea, M. Intrinsic viscosity and conformational parameters of xanthan in aqueous solutions: Salt addition effect. *Colloids Surf., B* **2014**, *122*, 512−519.
(79) Eich, A.; Wolf, B. A. Intrinsic Viscosities of Polyelectrolytes: Determination and Modeling of the Effects of Extra Salt. *ChemPhysChem* **2011**, *12*, 2786−2790.
(80) Xiong, X.; Wolf, B. A. Intrinsic viscosities of polyelectrolytes: specific salt effects and viscometric master curves. *Soft Matter* **2014**, *10*, 2124−2131.
(81) Tanahatoe, J. J.; Kuil, M. E. Dynamic Light Scattering of a Flexible Highly Charged Polyelectrolyte in the Dilute Concentration Regime. *Macromolecules* **1997**, *30*, 6102−6106.
(82) Odijk, T. Polyelectrolytes near the rod limit. *J. Polym. Sci., Polym. Phys. Ed.* **1977**, *15*, 477−483.
(83) Rushing, T. S.; Hester, R. D. Semi-empirical model for polyelectrolyte intrinsic viscosity as a function of solution ionic strength and polymer molecular weight. *Polymer* **2004**, *45*, 6587−6594.
(84) Lopez, C. G.; Horkay, F.; Mussel, M.; Jones, R. L.; Richtering, W. Screening lengths and osmotic compressibility of flexible polyelectrolytes in excess salt solutions. *Soft Matter* **2020**, *16*, 7289−7298.
(85) Spiteri, M. N.; Boué, F.; Lapp, A.; Cotton, J. P. Persistence Length for a PSSNa Polyion in Semidilute Solution as a Function of the Ionic Strength. *Phys. Rev. Lett.* **1996**, *77*, 5218−5220.
(86) Atashrouz, S.; Zarghampour, M.; Abdolrahimi, S.; Pazuki, G.; Nasernejad, B. Estimation of the Viscosity of Ionic Liquids Containing Binary Mixtures Based on the Eyring's Theory and a Modified Gibbs Energy Model. *J. Chem. Eng. Data* **2014**, *59*, 3691−3704.
(87) Canongia Lopes, J. N.; Costa Gomes, M. F.; Husson, P.; Pádua, A. A. H.; Rebelo, L. P. N.; Sarraute, S.; Tariq, M. Polarity, Viscosity, and Ionic Conductivity of Liquid Mixtures Containing [C4C1im]-[Ntf2] and a Molecular Component. *J. Phys. Chem. B* **2011**, *115*, 6088−6099.
(88) Roosta, A.; Bardool, R. A Simple Correlation for Estimating the Viscosity of Pure Ionic Liquids and Their Binary Mixtures. *Ind. Eng. Chem. Res.* **2017**, *56*, 4600−4610.
(89) Huang, M.-M.; Jiang, Y.; Sasisanker, P.; Driver, G. W.; Weingärtner, H. Static Relative Dielectric Permittivities of Ionic Liquids at 25 °C. *J. Chem. Eng. Data* **2011**, *56*, 1494−1499.
(90) Haynes, W. M. *CRC Handbook of Chemistry and Physics*; CRC press, 2014.
(91) Stoppa, A.; Hunger, J.; Hefter, G.; Buchner, R. Structure and Dynamics of 1-N-Alkyl-3-N-Methylimidazolium Tetrafluoroborate + Acetonitrile Mixtures. *J. Phys. Chem. B* **2012**, *116*, 7509−7521.
(92) Schrag, J. L.; Stokich, T. M.; Strand, D. A.; Merchak, P. A.; Landry, C. J. T.; Radtke, D. R.; Man, V. F.; Lodge, T. P.; Morris, R. L.; Hermann, K. C.; Amelar, S.; Eastman, C. E.; Smeltzly, M. A. Local modification of solvent dynamics by polymeric solutes. *J. Non-Cryst. Solids* **1991**, *131−133*, 537−543.
(93) Lodge, T. P. Solvent dynamics, local friction, and the viscoelastic properties of polymer solutions. *J. Phys. Chem.* **1993**, *97*, 1480−1487.
(94) Lodge, T. P.; McLeish, T. C. B. Self-Concentrations and Effective Glass Transition Temperatures in Polymer Blends. *Macromolecules* **2000**, *33*, 5278−5284.
(95) Savin, D. A.; Larson, A. M.; Lodge, T. P. Effect of composition on the width of the calorimetric glass transition in polymer-solvent and solvent-solvent mixtures. *J. Polym. Sci., Part B: Polym. Phys.* **2004**, *42*, 1155−1163.
(96) Takada, A.; Imaichi, K.; Kagawa, T.; Takahashi, Y. Abnormal Viscosity Increment Observed for an Ionic Liquid by Dissolving Lithium Chloride. *J. Phys. Chem. B* **2008**, *112*, 9660−9662.
(97) Tong, J.; Wu, S.; von Solms, N.; Liang, X.; Huo, F.; Zhou, Q.; He, H.; Zhang, S. The Effect of Concentration of Lithium Salt on the Structural and Transport Properties of Ionic Liquid-Based Electrolytes. *Front. Chem.* **2020**, *7*, 945.
(98) Rosol, Z. P.; German, N. J.; Gross, S. M. Solubility, ionic conductivity and viscosity of lithium salts in room temperature ionic liquids. *Green Chem.* **2009**, *11*, 1453−1457.
(99) Nakagawa, H.; Izuchi, S.; Kuwana, K.; Nukuda, T.; Aihara, Y. Liquid and Polymer Gel Electrolytes for Lithium Batteries Composed of Room-Temperature Molten Salt Doped by Lithium Salt. *J. Electrochem. Soc.* **2003**, *150*, A695.
(100) Garcia, B.; Lavallée, S.; Perron, G.; Michot, C.; Armand, M. Room temperature molten salts as lithium battery electrolyte. *Electrochim. Acta* **2004**, *49*, 4583−4588.
(101) Ferry, J. D. *Viscoelastic Properties of Polymers*, 3rd ed; John Wiley & Sons, 1980.
(102) Okada, Y.; Goto, Y.; Tanaka, R.; Katashima, T.; Jiang, X.; Terao, K.; Sato, T.; Inoue, T. Viscoelastic Properties of Tightly Entangled Semiflexible Polymer Solutions. *Macromolecules* **2018**, *51*, 9626−9634.
(103) Schweins, R.; Hollmann, J.; Huber, K. Dilute solution behaviour of sodium polyacrylate chains in aqueous NaCl solutions. *Polymer* **2003**, *44*, 7131−7141.
(104) Hayashi, K.; Tsutsumi, K.; Norisuye, T.; Teramoto, A. Electrostatic Contributions to Chain Stiffness and Excluded-Volume Effects in Sodium Hyaluronate Solutions. *Polym. J.* **1996**, *28*, 922−928.

https://doi.org/10.1021/acs.macromol.1c00576
Macromolecules 2021, 54, 5648−5661